

Prepared for publication in the *Astrophysical Journal*

The Baldwin Effect and Black Hole Accretion: A Spectral Principal Component Analysis of a Complete QSO Sample

Zhaohui Shang,¹ Beverley J. Wills,¹ Edward L. Robinson,¹ D. Wills,¹
Ari Laor,² Bingrong Xie,³ and Juntao Yuan¹

ABSTRACT

We have performed a spectral principal component analysis (SPCA) for an essentially complete sample of 22 low redshift QSOs with spectral data from Ly α to H α . SPCA yields a set of independent principal component spectra, each of which represents a set of relationships among QSO continuum and line properties. We find three significant principal components, which account for $\sim 78\%$ of the total intrinsic variance. The first component, carrying $\sim 41\%$ of the intrinsic variance, represents Baldwin relationships – anti-correlations between equivalent width of broad emission lines and continuum luminosity. The narrow line core (FWHM ~ 2000 km s $^{-1}$) of the broad emission lines dominate this component. The second component, accounting for $\sim 23\%$ of the intrinsic variance, represents the variations in UV continuum slope, which is probably the result of dust reddening, with possible contributions from starlight. The third principal component is directly related to the Boroson & Green “Eigenvector 1” (their first principal component), clearly showing the anti-correlation between strengths of optical Fe II and [O III] $\lambda 5007$, and other relationships previously found in the H β – [O III] region. This third component shows the expected strong correlation with soft X-ray spectral index. The widths of C III] $\lambda 1909$, Mg II $\lambda 2798$, and Balmer emission lines are also involved and clearly correlated, relating this component to black hole mass or Eddington accretion ratio. We find an inverse correlation between the strengths of the UV and optical Fe II blends, as suggested by some photoionization models. We also find correlations of the strengths of several low-ionization UV lines with Fe II(opt), and a strong positive correlation of C IV $\lambda 1549$ with [O III] strength. The wide wavelength coverage of our data enable us to see clearly the relationships between the UV and optical spectra of QSOs. The Baldwin effect and Boroson & Green’s Eigenvector 1 relationship are clearly independent. We demonstrate how Baldwin relationships can be derived using our first principal component, virtually eliminating the scatter caused by the third principal component. This rekindles the hope that the Baldwin relationships can be used for cosmological study.

Subject headings: galaxies: active — galaxies: nuclei — quasars: emission lines — ultraviolet: galaxies

¹Department of Astronomy, University of Texas at Austin, Austin, TX 78712. shang@astro.as.utexas.edu, bev@astro.as.utexas.edu, elr@astro.as.utexas.edu

²Department of Physics, Technion-Israel Institute of Technology, Haifa, 32000, Israel.

³Department of Physics & Astronomy, Rutgers University, Piscataway, NJ 08854.

1. INTRODUCTION

QSOs probe the universe at the epoch of galaxy formation. Their strong, broad emission lines arise predominantly from photoionization of high speed gas (10^3 km s^{-1} to 10^4 km s^{-1}) at 10^2 to 10^4 gravitational radii from a supermassive black hole ($\sim 10^8 M_\odot$). The emission line spectrum therefore promises to reveal the accretion mechanism, the origin of the fuel, and links with the host galaxy evolution. In addition, Baldwin (1977) discovered a relationship between line equivalent width and luminosity, suggesting that the luminosity may be determined directly from the spectrum, hence providing an important test of cosmological models at high redshift, z . Forty years after QSOs’ discovery, these promises have yet to be fulfilled. There are two main, related, reasons for this. (i) Even in the nearby lower-luminosity AGN, the broad line region (BLR) remains unresolved and its structure can be inferred only indirectly. For example, reverberation mapping has shown that light-travel times from the central continuum source increase with decreasing ionization (from a few light days, to light months, e.g., Netzer & Peterson 1997). Emission line strengths and the fact that absorption along the line-of-sight to the continuum source occurs only sometimes, show that only a few percent of the center is covered by BLR gas, and the global filling factor is very small. (ii) To first order, emission-line ratios of all UV-optically selected QSOs are surprisingly similar. Baldwin et al. (1995) successfully reproduced the average QSO spectrum – showing that their similarity was the result of powerful selection. Given a BLR with a wide range of gas density, column density and ionizing flux, different emission lines are formed predominantly in gas with different physical conditions optimal for their formation. Thus the integrated line properties of the BLR spectrum are quite insensitive to the density, ionization, and column density of BLR gas. This is true of any BLR model that exhibits a range of density at each radius; thus the integrated properties of the BLR cannot clearly distinguish among multi-cloud models (Baldwin et al. 1995; Bottorff & Ferland 2001), disk-wind models (Murray & Chiang 1997), stellar wind, or bloated stellar atmosphere models (e.g., Scoville & Norman 1988; Alexander & Netzer 1994).

In important details, however, spectra of QSOs are not all similar. Rather than comparing models with average line profiles and line ratios, we can learn more from direct observations of the dependence of QSO spectra on observed parameters that may be related directly to the central engine. These dependences, including velocity information across the broad line profiles, provide a powerful tool that has yet to be fully exploited. Two striking sets of relationships have been found, relating QSOs’ optical – UV emission lines and soft X-ray continua with fundamental properties of the central engine. One is the Baldwin relationship between equivalent widths of emission lines from the BLR, and the luminous power output, L . The other set is the “Principal Component 1” (also called “Eigenvector 1”) relationships, which appear to be related to the Eddington ratio. These relationships may allow us to explore the accretion history of QSOs and, ultimately, the formation of galaxy spheroids.

The Baldwin effect is an inverse relationship between the equivalent widths of QSOs’ broad emission lines EW , and the UV continuum luminosity L , $EW \propto L^\beta$, spanning 7 orders of magnitude in luminosity. It was originally derived using the C IV $\lambda 1549$ line (Baldwin 1977; Baldwin, Wampler, & Gaskell 1989), and the continuum luminosity at 1549 \AA . Other lines show Baldwin relationships (e.g., Kinney, Rivolo, & Koratkar 1990, Espey & Andreadis 1999), with $\beta = -0.05$ to -0.3 , the slope apparently increasing with increasing ionization potential. The “line cores” (emission from low velocity gas) contribute more than the line wings (Francis et al. 1992 – hereinafter, FHFC; Osmer, Porter, & Green 1994; Francis & Koratkar 1995; Brotherton & Francis 1999). It has been suggested that the Baldwin effect results from a luminosity-dependent spectral energy distribution, ionization parameter, covering factor, or is the result of inclination (Peterson 1997; Korista 1999; Ferland & Baldwin 1999). The original hope was that QSO luminosity could be determined from line equivalent widths, and that the resulting $L - z$ relationship could be used to discriminate among

cosmological models. However, so far, observed Baldwin relationships show too much scatter.

In a Principal Component Analysis (PCA) of direct, integrated, line measurements in the $H\beta$ region of 87 low z QSOs, Boroson & Green (1992, hereinafter, BG92) discovered that most of the spectrum-to-spectrum variance, represented by the first principal component (Eigenvector 1, hereinafter, BG PC1), links a number of variables: decreasing broad $H\beta$ line width corresponds to stronger Fe II optical emission (Fe II(opt)), weaker [O III] $\lambda 5007$ emission, and increasing $H\beta$ asymmetry from stronger red to stronger blue wings. BG92 suggested that the Fe II(opt) – [O III] anticorrelation arose from an increase in covering factor of dense Fe II-emitting gas, resulting in an increase in the Eddington accretion ratio. The case for higher Eddington ratios was especially supported by the Laor et al. (1994, 1997, hereinafter, L94, L97) inclusion of X-ray spectral index α_x in this principal component: steeper α_x corresponds to narrower $H\beta$ etc. In a virial interpretation of $H\beta$ width, narrower $H\beta$ would correspond to smaller black-hole mass, hence higher Eddington ratio; steeper α_x corresponds to higher Eddington ratios as inferred for Galactic black hole candidates (Pounds, Done, & Osborne 1995). Also using a PCA on integrated line measurements, Wills et al. (1999a) showed that these relationships extend to the UV: stronger Fe II(opt) corresponds to a larger ratio Si III] $\lambda 1892$ /C III] $\lambda 1909$ indicating higher densities, also weaker C IV $\lambda 1549$, stronger N V $\lambda 1240$, stronger Si IV+O IV] $\lambda 1400$ feature, and other properties. The support for a virial interpretation of $H\beta$ line widths has further strengthened the case for an Eddington ratio interpretation of these BG PC1 relationships (Boroson 2002, hereinafter, B02)

The discovery of supermassive black holes in nearby massive galaxies (Kormendy & Ho 2000) and the proportionality between M_{bh} and spheroid masses (Ferrarese & Merritt 2000; Gebhardt et al. 2000) has allowed the calibration of virial masses in nearby QSOs and active galaxies (Laor 1998; Gebhardt et al. 2000). Thus, the velocity width of the broad $H\beta$ emission line, and a nuclear distance for the $H\beta$ -emitting gas derived from reverberation mapping or photoionization modeling (Wandel, Peterson, & Malkan 1999; Kaspi et al. 2000), allow the measurement of M_{bh} , hence the calculation of the maximum (Eddington) accretion luminosity, L_{Edd} , and the Eddington accretion ratio, L/L_{Edd} . Comparison of the space density of local black holes with that of QSOs at the peak of their luminous output near $z \sim 2 - 3$, shows that nearby galaxies harbor the black-hole relics of QSO activity (e.g., Marconi & Salvati 2002; Fabian 1999; Gilli, Salvati, & Hasinger 2001). Together with the M_{bh} – spheroid mass relationship this then points to an interrelated evolutionary history for QSOs and massive galaxies (e.g., Fabian 1999; Silk & Rees 1998). Thus an understanding of the above Principal Component relationships is important for understanding galaxy evolution.

In this paper we extend the above analyses, carrying out a spectral Principal Component Analysis (SPCA) on the essentially complete sample of optical-UV spectra of 22 QSOs, the same sample that we used for the PCA on integrated line measurements described above.

We briefly describe the sample, observations and reductions in §2. In §3 we describe the technique of spectral PCA. The results of the SPCA are presented in §4. We first reproduce the main results of the BG92 PCA to illustrate the power of SPCA. The principal component spectra covering the Ly α to H α region give a striking visual impression of the relationships among optical and UV emission lines of different ionization stage and critical density. Such broad band coverage is essential for investigating relationships involving broad-band features such as the entire optical-UV spectral energy distribution, the Balmer continuum and the blended Fe II(UV) emission (“small blue bump”). We include some SPCA simulations to illustrate the non-linear effects of line profile relationships. In §5 we discuss the distinctness and separation of the emission-line spectral components, and the interpretation of the “intermediate line region” and “very broad line region” as presented by Francis, Brotherton, and collaborators. We summarize our results in §6, mentioning some implications for future research, in particular, the usefulness of SPCA for reducing scatter in Baldwin

relationships, and in tracking the evolution of Eddington ratios in QSOs. Complementary analyses for our QSO sample, including results of PCA on direct, integrated, parameters, have been presented by Wills et al. (1999a), Francis & Wills (1999), Wills et al. (1999b,c), & Wills, Shang, & Yuan (2000).

2. OBSERVATIONS AND DATA REDUCTION

We have observed optical-UV spectra for 22 of the 23 PG QSOs making up the complete optically selected sample investigated by L94 and L97. Laor et al. selected all QSOs from the Bright Quasar Survey (BQS) (Schmidt & Green 1983) with redshift $z < 0.4$ and a Galactic hydrogen column density $N_{\text{HI}} < 1.9 \times 10^{20} \text{ cm}^{-2}$. This sample should be representative of low-redshift, optically selected QSOs, but subject to the same incompleteness as the BQS (Wampler & Ponz 1985; Goldschmidt et al. 1992; Mickaelian et al. 2001). The QSOs in the sample are listed in Table 1 along with their redshifts, magnitudes, and other parameters. The low redshift ensures observational access to the soft X-rays nearest the wavelength of the ionizing continuum. The low Galactic absorption and brightness of this low redshift sample enable accurate determination of the intrinsic soft X-ray and UV spectra. In addition the low redshift and UV coverage allows investigation of the Ly α region, with much reduced confusion from intergalactic absorption lines.

For the ultraviolet region, we obtained *Hubble Space Telescope* (HST) Faint Object Spectrograph (FOS) spectrophotometry for 16 QSOs and used archival FOS data for 6 QSOs, covering wavelengths from below Ly α to beyond the atmospheric cutoff near 3200 Å in the observed frame⁴. Instrumental resolution is equivalent to $\sim 230 \text{ km s}^{-1}$ (FWHM). The FOS pipeline calibration is described at <http://www.stecf.org/poa/FOS/index.html>.

Optical data were obtained at McDonald Observatory, generally with the Large Cassegrain Spectrograph on the Harlan J. Smith 2.7m telescope, supplemented by some from the HST FOS. We were usually able to get quasi-simultaneous optical observations, within a month of the new HST observations, to reduce the uncertainty caused by QSO intrinsic variability. Observations were made through narrow (1''– 2'') and wide (8'') slits. Standard stars were observed several times each night. They were chosen from the spectral standard stars for HST calibration (Bohlin 1996, 2000) to ensure consistent calibration between UV and optical data. Usually 2–3 spectra for each object are required to cover wavelength ranges from below 3200 Å to beyond H α . Instrumental resolution for the optical spectra is $\sim 7 \text{ Å}$ FWHM, equivalent to 450 km s^{-1} to $\sim 250 \text{ km s}^{-1}$ (FWHM) in the H β to H α region.

Higher resolution spectra ($\sim 180 \text{ km s}^{-1}$ FWHM) of the Fe II(opt)–H β –[O III] region were obtained with the same spectrograph and telescope at McDonald Observatory and are used only to determine the redshifts of most of the sample QSOs with sufficiently strong [O III] lines.

Standard packages in IRAF were used to reduce the data. Wavelength calibration was done by using comparison spectra. For some spectra, it was necessary to shift the wavelength scale to match the wavelengths of night sky lines. Spectrophotometric calibration was achieved by: 1) using standard star spectra to calibrate QSO spectra to an absolute flux-density scale, 2) scaling the narrow slit QSO spectra to match the shape and absolute flux-density level of the wide slit QSO spectra. The photometric accuracy is $\sim 5\%$.

UV and optical spectra for each object were then combined in the observed frame. Before combination, some spectra were scaled by a few percent to match, in the overlap region, the continuum level of the

⁴We were not able to obtain the UV spectrum of PG1543+489 between 1648 Å and 2446 Å (rest frame). Also its optical spectral data miss part of the H α red wing.

Table 1. The Sample

| Object | z^a | m_B^b | α_x^c | FWHM(H β) ^c (km s ⁻¹) | $L_\nu(1549)^d$ (erg s ⁻¹ Hz ⁻¹) | W_{SPC1}^e | W_{SPC2}^e | W_{SPC3}^e |
|------------|---------------------|---------|--------------|--|--|---------------------|---------------------|---------------------|
| PG0947+396 | 0.2056 | 16.40 | -1.510 | 4830 | 30.33 | 3.67 | -2.73 | -1.65 |
| PG0953+414 | 0.2341 | 15.05 | -1.570 | 3130 | 30.59 | 7.31 | -0.99 | -0.88 |
| PG1001+054 | 0.1603 ^f | 16.13 | -2.800 | 1740 | 29.73 | ... | ... | ... |
| PG1114+445 | 0.1440 | 16.05 | -0.880 | 4570 | 29.80 | ... | ... | ... |
| PG1115+407 | 0.1541 | 16.02 | -1.890 | 1720 | 30.08 | -2.37 | -6.06 | 2.46 |
| PG1116+215 | 0.1759 | 15.17 | -1.730 | 2920 | 30.67 | -2.21 | -2.55 | 0.66 |
| PG1202+281 | 0.1651 | 15.02 | -1.220 | 5050 | 29.51 | ... | ... | ... |
| PG1216+069 | 0.3319 | 15.68 | -1.360 | 5190 | 30.69 | -0.22 | 7.96 | -2.26 |
| PG1226+023 | 0.1575 | 12.86 | -0.942 | 3520 | 31.37 | -8.39 | -1.79 | 2.19 |
| PG1309+355 | 0.1823 | 15.45 | -1.510 | 2940 | 30.21 | -10.15 | 7.36 | -0.67 |
| PG1322+659 | 0.1675 | 15.86 | -1.690 | 2790 | 30.02 | 6.48 | 3.63 | -0.27 |
| PG1352+183 | 0.1510 | 15.71 | -1.524 | 3600 | 30.04 | 2.98 | -4.26 | -0.67 |
| PG1402+261 | 0.165 ^g | 15.57 | -1.930 | 1910 | 30.40 | -1.19 | -4.59 | 3.62 |
| PG1411+442 | 0.0895 | 14.99 | -1.970 | 2670 | 29.56 | ... | ... | ... |
| PG1415+451 | 0.1143 | 15.74 | -1.740 | 2620 | 29.72 | 6.80 | 3.92 | 2.16 |
| PG1425+267 | 0.3637 ^f | 15.67 | -0.940 | 9410 | 30.42 | -5.01 | 1.29 | -6.59 |
| PG1427+480 | 0.2203 | 16.33 | -1.410 | 2540 | 30.20 | 7.94 | -1.50 | -2.84 |
| PG1440+356 | 0.0773 | 15.00 | -2.080 | 1450 | 29.90 | 7.33 | 6.16 | 7.71 |
| PG1444+407 | 0.267 ^g | 15.95 | -1.910 | 2480 | 30.63 | -9.49 | 1.75 | 2.32 |
| PG1512+370 | 0.3700 ^f | 15.97 | -1.210 | 6810 | 30.66 | -0.02 | -0.03 | -7.01 |
| PG1543+489 | 0.400 ^g | 16.05 | -2.110 | 1560 | 30.75 | -6.27 | -2.96 | 2.83 |
| PG1626+554 | 0.1317 | 16.17 | -1.940 | 4490 | 30.11 | 2.81 | -4.61 | -1.12 |

^aFrom measurements of [O III] after removing Fe II emission in our separate higher resolution spectra unless noted

^bFrom Schmidt & Green (1983)

^cFrom Laor et al. (1997). α_x is soft X-ray spectral index.

^dContinuum luminosity at 1549Å, from measurements of our UV spectra. We use $H_0 = 50$ km s⁻¹Mpc⁻¹, and $q_0 = 0.5$.

^eWeights of principal components from the SPCA of 18 spectra covering Ly α to H α in §4.

^fFrom measurements of [O III] in the spectra of this study. Fe II emission was not removed.

^gFrom measurements of H β and other emission lines in the spectra of this study. These objects have very weak [O III].

spectrum with the best flux-density calibration, usually the HST spectra. Galactic reddening was removed using the H I column densities N_{HI} from accurate 21 cm data (references in L94, L97) and an empirical relationship $N_{\text{HI}} = 53 \times 10^{20} E(B-V) \text{ cm}^{-2}$ (Predehl & Schmitt 1995). The column densities are low with uncertainties of $\pm 10^{19} \text{ cm}^{-2}$, insuring small corrections for Galactic absorption, especially in the UV. The error in flux density introduced by this correction is less than 2% even at the shortest wavelengths. The dominant uncertainty in flux density arises from the scatter in the $N_{\text{HI}} - E(B-V)$ relationship, and is $\sim 12\%$ in the worst case, but generally significantly less.

After subtraction of optical Fe II emission blends with the same Fe II template and method used by BG92, we used the higher resolution spectra to define a rest-frame wavelength scale referred to a wavelength of 5006.8 Å for [O III] and applied the redshift to the combined spectra. Redshifts for other QSOs were obtained from the lower resolution spectra in this study (Table 1). We present our combined spectra in Fig. 1.

3. SPECTRAL PRINCIPAL COMPONENT ANALYSIS

Principal component analysis (PCA) is a powerful tool for multivariate analysis. Given a sample of n QSOs, each with p measured variables, x_i (e.g., line width, luminosity, soft X-ray spectral index α_x , etc.), PCA defines a set of p new orthogonal variables PC_j . The PC_j are linear combinations of the original variables:

$$\text{PC}_j = \sum_{i=1}^p a_{ij} x_i \quad (1)$$

ordered according to the fraction of the total sample variance accounted for by each PC_j , e.g., PC_1 accounts for more variance than any other, PC_2 accounts for the next largest amount of variance, etc.. If there are strong linear relationships among the original variables, each of these relationships will be represented by a principal component, and fewer principal components will be required to describe the total variation among QSOs, thus providing a simpler description of the dataset. If the measured variables are unrelated, there will still be p PC_j s; but no simplification will result; nothing will have been accomplished. The hope is that any PC_j accounting for a significant fraction of the total sample variance might be related to one or more underlying fundamental physical parameters, giving some physical insight into the cause of the variations (see BG92, B02). The PCA technique is explained in more detail and applied to integrated, direct, measurements of the present sample of 22 spectra, by Francis & Wills (1999) and Wills et al. (1999b).

In spectral PCA (SPCA), the whole spectrum is divided into p small wavelength bins, and each input variable x_i is the flux in the i th wavelength bin. The j th principal component from this analysis can be represented as spectra of the coefficients a_{ij} of each x_i (see §4). Features of the same sign in the a_{ij} spectrum are positively correlated, while those with opposite sign are anticorrelated. One of the advantages of SPCA is that correlations can be investigated without parameterizing the line profiles or defining the continua. In addition, unlike the “composite spectrum analysis” which shows average QSO properties, the SPCA analysis keeps the information for individual QSOs, e.g., the weights of the principal component spectra for each QSO (Table 1). The original (normalized) spectra in the sample can therefore be reconstructed by adding the weighted principal component spectra to the mean spectrum. The SPCA technique is described in more detail by FHFC and references therein.

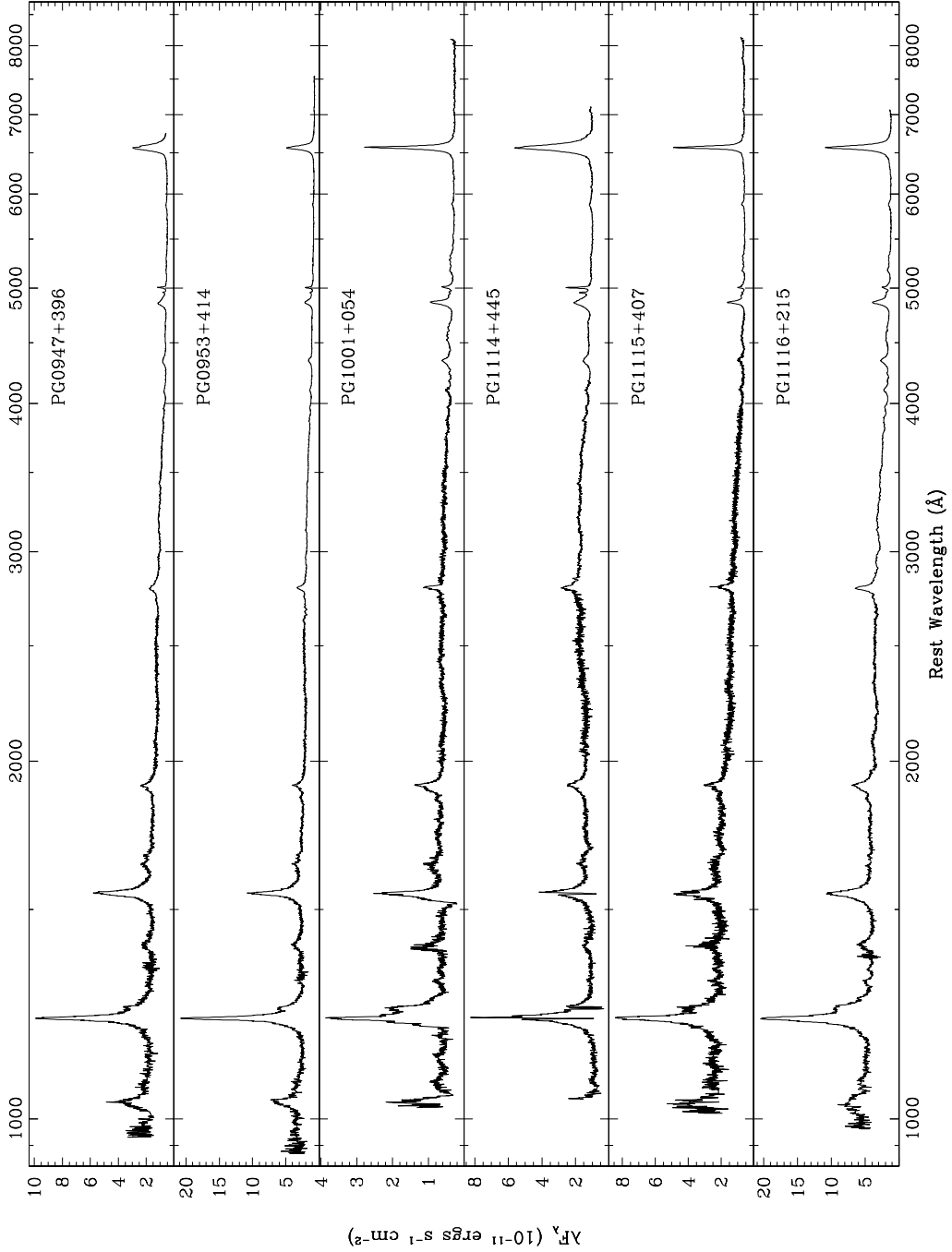


Fig. 1.— Combined rest-frame UV-optical spectra of the QSOs in our sample. Galactic absorption lines are removed except for some in the far UV. Galactic reddening is also removed.

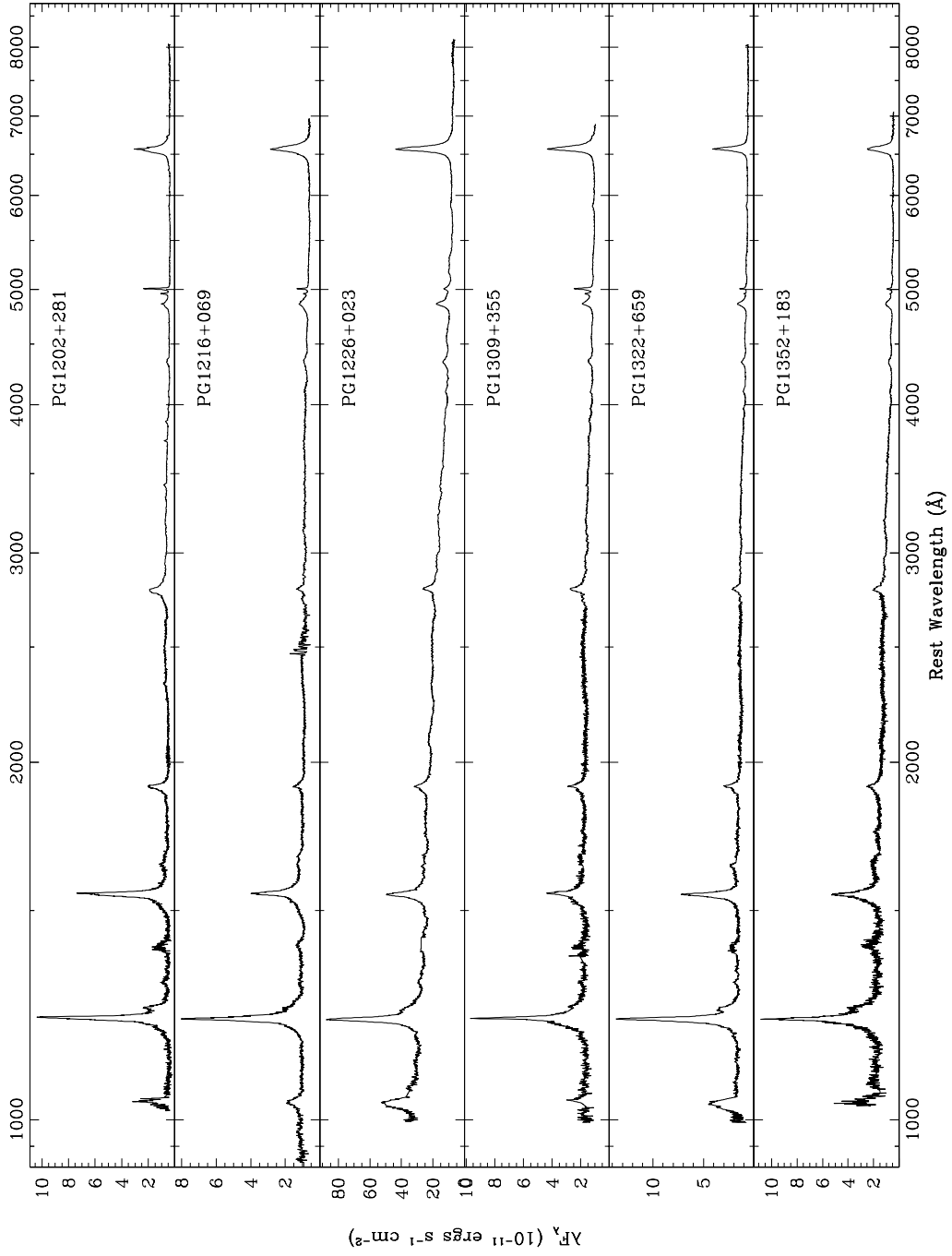


Fig. 1.— Continued

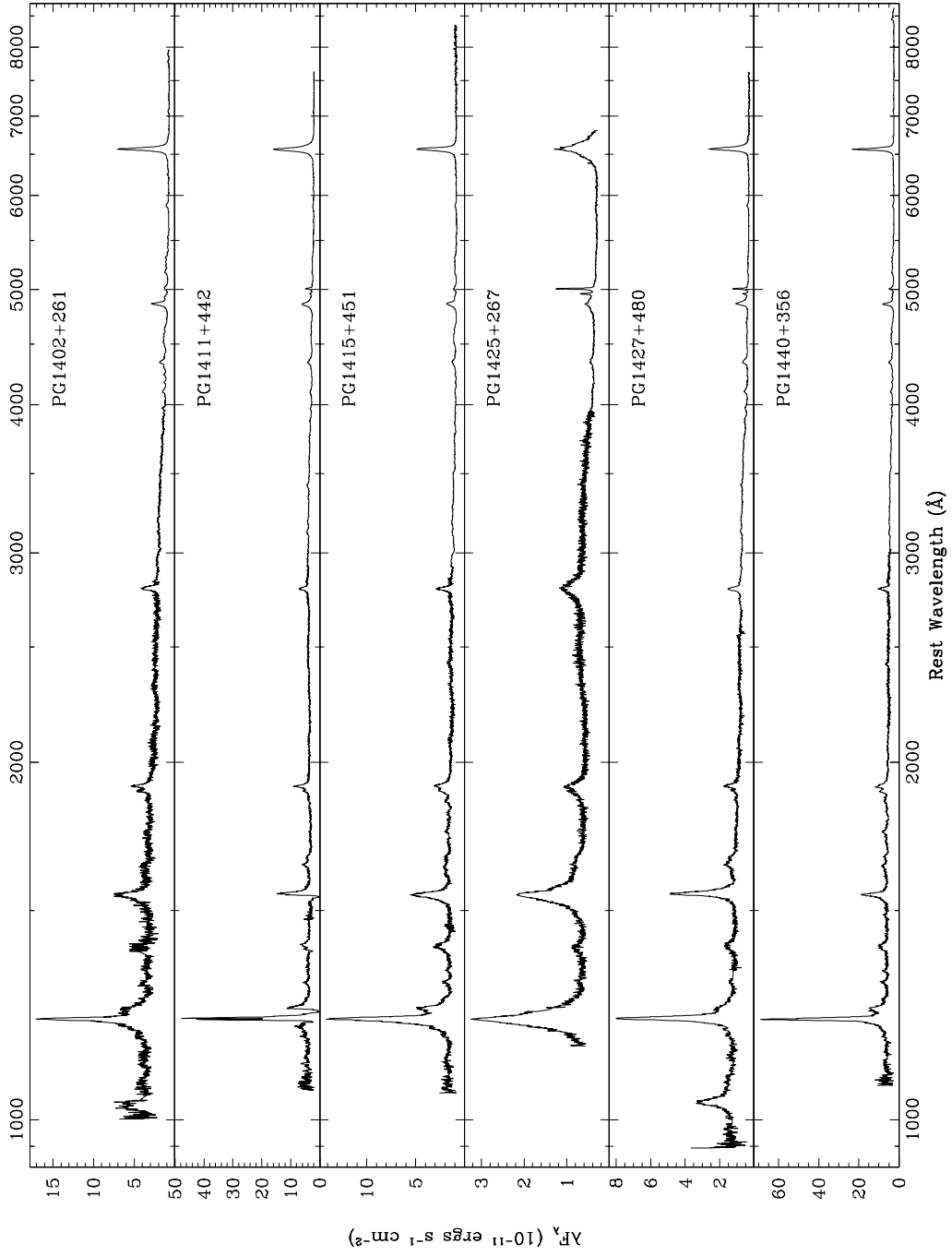


Fig. 1.— Continued

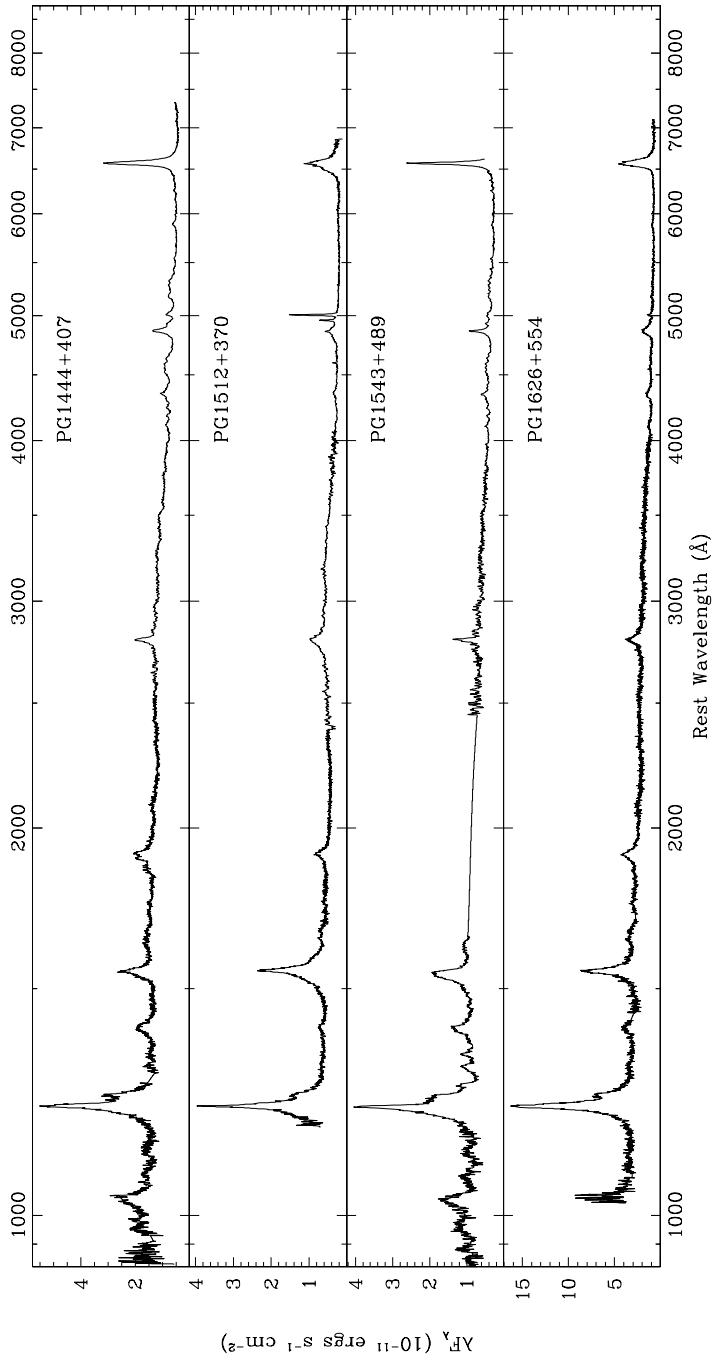


Fig. 1.— Continued

We have rebinned the rest-frame spectra in equal logarithmic wavelength intervals, representing equal intervals in velocity space. Individual spectra are first normalized by their mean flux density; this means that the resultant principal component spectra represent flux density variations relative to this mean – for emission lines the integral over the line in the principal component spectra represents essentially equivalent width variations. Next, the mean and standard deviation spectra are formed, and the mean spectrum subtracted from each QSO spectrum. This is equivalent to moving the dataset to the origin of the multidimensional space represented by the x_i . We used the code developed by FHFC (<http://www.mso.anu.edu.au/~pfrancis/>). The resulting principal components are ordered according to the fraction of the total sample variance that they account for.

4. RESULTS

We first apply SPCA to our sample in the $H\beta$ region and compare the results (Fig. 2) with the well known BGPC1. As expected, the strong anticorrelation between [O III] $\lambda 5007$ and Fe II appears in the first principal component, indicated by the oppositely directed [O III] and Fe II features. The “W” shape of $H\beta$ in the first principal component indicates that the width of $H\beta$ increases with increasing [O III] equivalent width (see §4.5 for simulations). The second principal component shows that the equivalent widths of the Balmer lines are correlated with each other and these lines are narrower than in the mean spectrum. Neither principal component is exactly equivalent to BG92’s principal components 1 and 2 because they used integrated line measurements and other parameters in their PCA analysis, such as absolute magnitude M_v and optical–X-ray spectral index α_{ox} .

We next apply SPCA to the sample over the wavelength range from $Ly\alpha$ to $H\alpha$. The three absorption-line QSOs (PG 1001+054, PG 1114+445 and PG 1411+442) and PG1202+281, which is an extreme object in the sample, are excluded from this analysis with broad wavelength coverage (for details, see §4.4). The results using 18 objects⁵ are presented here. The principal component spectra are shown in Fig. 3, where they are compared with the mean and standard-deviation spectra.

Compared with the mean spectrum, the standard deviation spectrum has stronger emission from low velocity gas. $H\beta$ shows a narrow component and a broad component with a stronger blue wing. The $Ly\alpha$ $\lambda 1216$ and N V $\lambda 1240$ lines are more clearly resolved than in the mean spectrum; similarly the Si III] $\lambda 1892$ and C III] $\lambda 1909$ emission lines. Mg II $\lambda 2798$ appears not to follow this pattern. Fe II emission near $H\beta$ shows some sharper features in the standard deviation spectrum than in the mean spectrum, indicating that Fe II emission also has different kinematic components. That the line cores contribute most to spectrum-to-spectrum variance has been noted before (e.g., FHFC; Brotherton et al. 1994a). The concave shape of the overall standard deviation spectrum arises simply from the dispersion of continuum slopes among individual spectra, because each is normalized by its mean flux density.

The total variance of the sample is the sum of the intrinsic variance and the variance from the observational and instrumental noise in the original spectra. We are interested in the intrinsic variance. We first estimate the contribution from noise, for each QSO spectrum. We create a noise spectrum by shifting the original spectrum by two pixels, form the difference spectrum of the two, remove sharp spikes around strong line features, and divide by $\sqrt{2}$. We then calculate the noise contribution to the variance by summing

⁵For PG 1543+489, we linearly interpolate the spectrum over the missing data from 1648 Å to 2446 Å. SPCA shows essentially the same results whether we include or exclude this object.

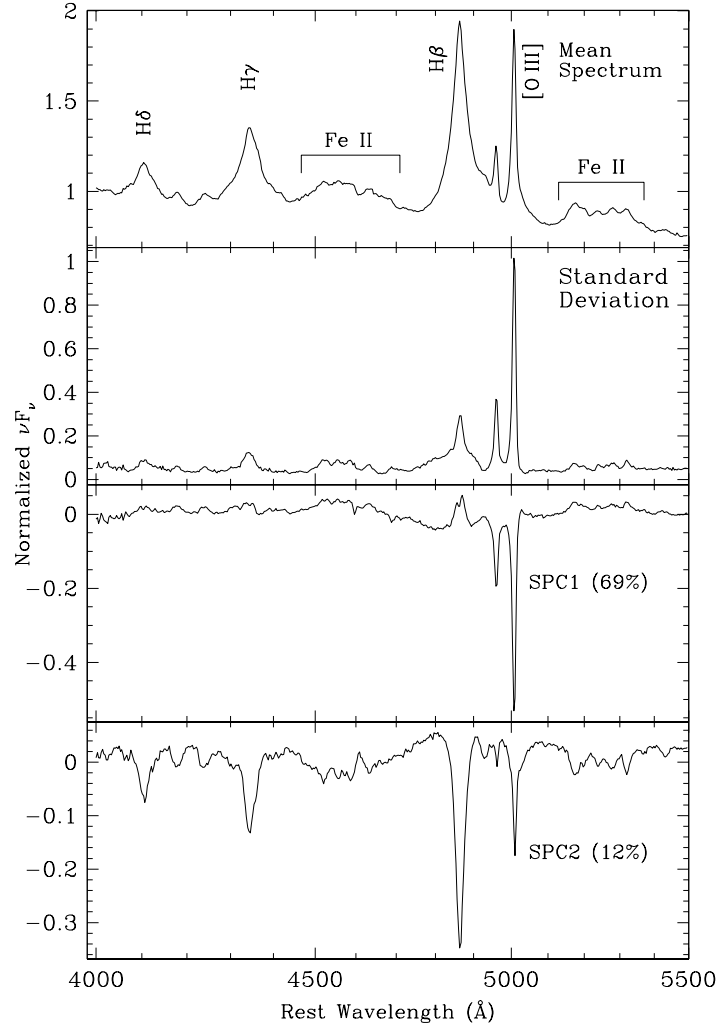


Fig. 2.— SPCA results in the $H\beta$ region for 22 QSOs. The ordinate is νF_ν , with each QSO spectrum normalized by its mean flux density. Features that extend in the same or opposite directions are positively or negatively correlated, respectively, in the SPC spectra. The first principal component is similar to the Boroson & Green (1992) first principal component. The “W” shape of $H\beta$ in SPC1 indicates the width increases with stronger $[O III]$ (§4.5). The second principal component shows the correlations of Balmer lines. The number in the parentheses indicates the percentage of the total intrinsic variance that each principal component accounts for (see §4). It shows that the first principal component is much more important than the second one in this region.

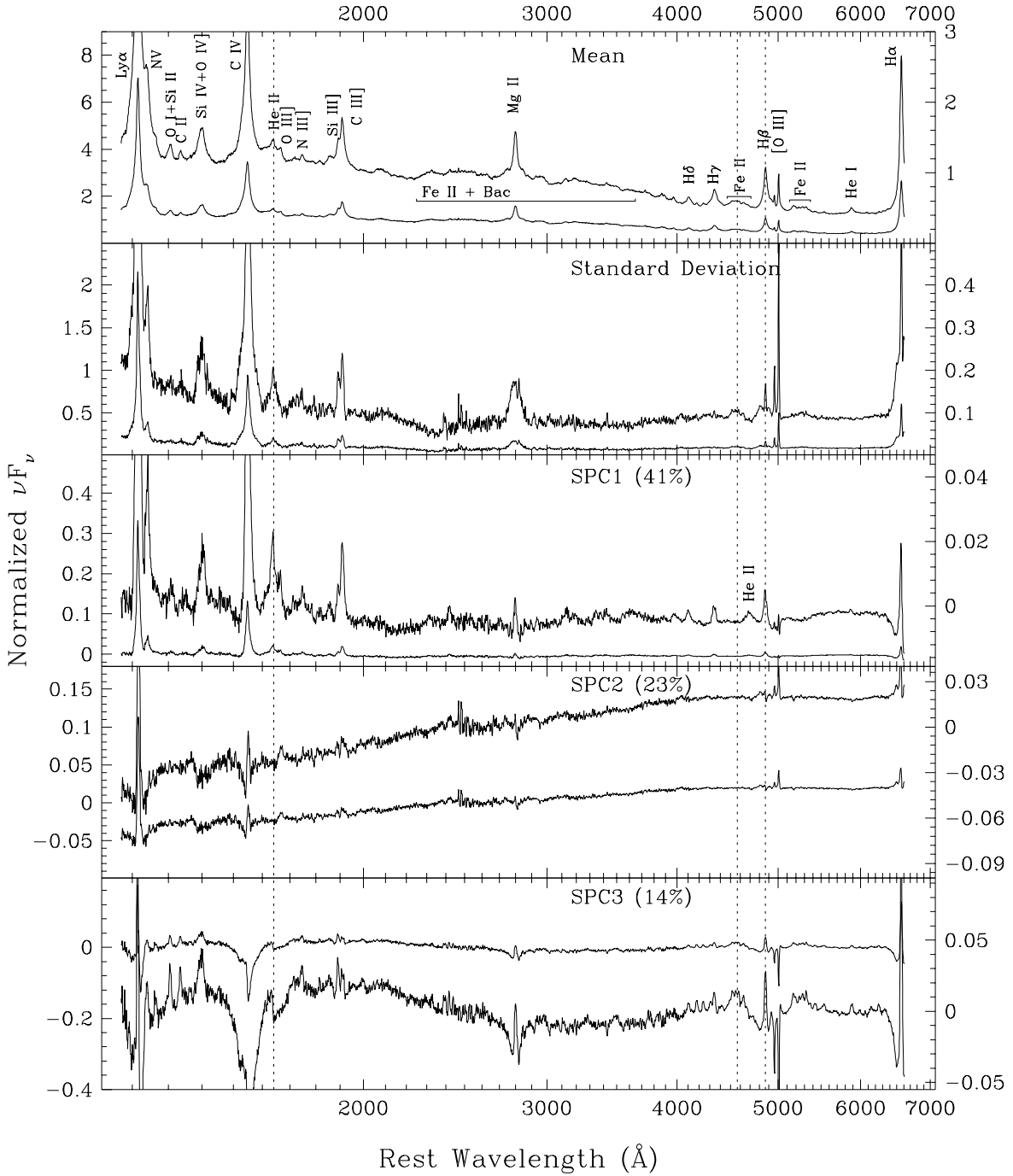


Fig. 3.— SPCA results for the UV-optical spectra of 18 QSOs. The numbers in parentheses are the percentages of the sample intrinsic variance that are accounted for by each principal component. Each panel presents the spectrum with the full ordinate range (left-hand scale), and scaled to show details of the weaker features (right-hand scale). The dashed vertical lines indicate the alignment at the He II $\lambda 1640$ feature, at the peak of the Fe II(opt) feature, and at H β .

the squares of the fluxes of each bin in the noise spectrum. We then calculate the total variance for each QSO spectrum, by summing the squares of the differences between that spectrum and the mean spectrum. Similarly we calculate the variance between each observed spectrum, and its reconstruction derived from the mean plus the principal component spectra appropriately weighted for that QSO. After removing the noise contribution, we calculate the fraction of the total intrinsic variance accounted for by the addition of each subsequent principal component, as described by FHFC. The results are summarized for the whole spectrum, the UV, and the 2100 Å – 6607.5 Å region, in Table 2. We find that the first, second, and third components account for 41%, 23%, and 14% of the total intrinsic variance, for a total of 78% of the intrinsic variance.

4.1. The First Principal Component: Emission-Line Cores

The most striking feature of the first principal component spectrum (Fig. 3, SPC1) is the correlation of the flux from gas of relatively low radial velocity (hereinafter “line-core component”). The widths (FWHM) of the emission line features in this component are given in Table 3, and are typically 2000 km s⁻¹ when corrected for blended doublets. By contrast He II λ4686 is very broad, with FWHM ≈ 4900 km s⁻¹. The peaks of these features are at the systemic redshift and are symmetric. Relative to these narrow profiles, the broad line profiles of the mean spectrum appear to have a blue-shifted “base”, at least for Lyα and C IV (Fig. 4) as noted in higher-redshift spectra by FHFC and Brotherton et al. (1994a).

The strength of broad He II λ4686 is correlated with that of the line cores (but absent in SPC3). The revealing of He II λ4686 in SPC1 is striking, because it is not obviously present in either the mean or standard deviation spectrum. We cannot exclude a broad He II λ1640 line corresponding to He II λ4686 as it is blended with narrower He II λ1640 and other emission lines. Emission from the broad Fe II UV and optical blends appears weak or absent.

In the UV, the line-core spectrum appears to be essentially the same as the first principal component of the SPCA analysis of 232 UV spectra of the Large Bright QSO Survey (LBQS) by FHFC. Francis & Koratkar (1995) followed up and confirmed the FHFC suggestion that this emission may be responsible for the Baldwin effect, by deriving the line-core equivalent width dependence on luminosity. This was demonstrated more qualitatively by Osmer et al. (1994), and Green (1998) also suggested this for Lyα and C IV. However these published studies cover only the strong UV lines between ~1150 Å and 2000 Å.

Is our SPC1 really the same as that for the LBQS, and does it depend on luminosity as expected for the Baldwin Effect? Fig. 5a and Table 4 show that the weight of this line-core component for each QSO is indeed anticorrelated with (logarithmic) L_ν(1549), the continuum luminosity at 1549 Å. For 18 QSOs, the Pearson and Spearman rank (two-tailed) probabilities of this correlation arising by chance from uncorrelated variables

Table 2: Fractional Component Contributions to the Total Intrinsic Variance

| Component(s) | Wavelength range (Å) | | |
|--------------|----------------------|-----------|-------------|
| | 1171–6607.5 | 1171–2100 | 2100–6607.5 |
| SPC1 | 0.41 | 0.49 | 0.08 |
| SPC2 | 0.23 | 0.18 | 0.44 |
| SPC3 | 0.14 | 0.13 | 0.20 |
| SPC3-10 | 0.31 | 0.29 | 0.41 |

Table 3: SPC1 and Mean Spectrum Line Widths

| Line | SPC1 | | Mean FWHM |
|----------------------------------|-------|-------------------------|-----------|
| | FWHM | corr. FWHM ^a | |
| Ly α | 1940 | ... | 2910 |
| N v $\lambda\lambda$ 1238,1242 | 3150 | 2911 | ... |
| C IV $\lambda\lambda$ 1548,1550 | 2390 | 2313 | 3680 |
| C III] λ 1909 | 2390 | ... | 4480 |
| Mg II $\lambda\lambda$ 2796,2803 | 1370: | 970: | 2860 |
| H δ | 2370: | ... | 2760 |
| H γ | 2250 | ... | 3400 |
| He II λ 4686 | 4880 | ... | ... |
| H β | 1680 | ... | 2600 |
| H α | 1440: | ... | 2300 |

Note – FWHMs (km s^{-1}) are estimated by directly measuring the widths between the half maxima of line profiles. Ly α and N v are not deblended in the mean spectrum, and He II λ 1640 cannot be measured there.

^aCorrected FWHM assume a 1:1 doublet intensity ratio for N v and C IV, 2:1 for Mg II.

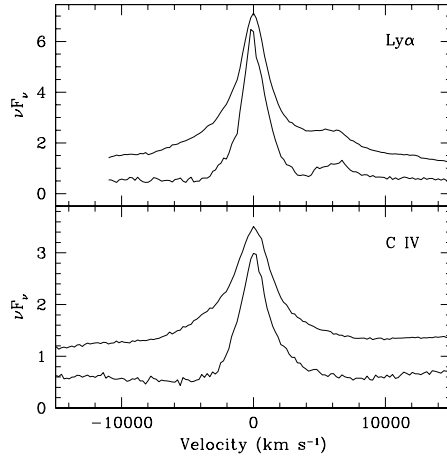


Fig. 4.— Comparison of SPC1 line profiles (lower spectra) with line profiles of the mean spectrum, showing the blueshifted bases in Ly α and C IV.

are 1.1% and 2.0%, respectively. We have redone the SPCA, including the extreme, low luminosity QSO PG 1202+281 (Fig. 5b) and these probabilities become 0.1% and 0.5%, respectively. A Bayesian analysis gives <27% and <7% probabilities of the correlation arising by chance for the two cases above. Since all the spectra are normalized, this is actually an anticorrelation between line equivalent width and luminosity. Wills et al. (1999a) reported, for the same sample, evidence of the Baldwin effect in the second principal component of their PCA analysis of direct line measurements that do not separate the narrow and broad components (Wills et al. 1999b & Francis & Wills 1999 give complementary details). We now see that the correlation they found was actually a correlation with the equivalent widths of the line-cores.

To test whether our correlation is actually consistent with Baldwin relationships found in the UV spectra of much larger samples, we measure the equivalent width of C IV from the SPCA results for 19 QSOs. $EW(C\text{ IV}) = (F_{\text{mean}} + W_{\text{SPC1}}F_{\text{SPC1}})/(C_{\text{mean}} + W_{\text{SPC1}}C_{\text{SPC1}})$, where F_{mean} and C_{mean} are the C IV flux and the flux density of the fitted local continuum in the mean spectrum, F_{SPC1} and C_{SPC1} are those in the first principal component spectrum, and W_{SPC1} is the weight of SPC1 for each QSO, evaluated from SPCA. We deblend the C IV region to exclude He II $\lambda 1640$ and O III] $\lambda 1664$ in the mean spectrum, and C IV is narrow enough to be separated from He II $\lambda 1640$ and O III] $\lambda 1664$ in SPC1. This procedure is equivalent to measuring the spectra reconstructed with only the mean spectrum and SPC1, and therefore includes the equivalent width variation of the line cores, but excludes scatter that would otherwise be introduced by orthogonal principal components. The filled circles in Fig. 6 show the anticorrelation between this $EW(C\text{ IV})$ and $L_{\nu}(1549)$. The slope of the least-squares fit is -0.18 ± 0.05 , which agrees with -0.16 ± 0.06 obtained by Kinney et al. (1990). This could be coincidence for our small sample with a luminosity range of only 1.6 dex, but it is more likely because we reduce the scatter in the luminosity relationship by using only the line core component. The open circles in Fig. 6 show the integrated equivalent widths of the C IV line measured directly from the original spectra (Francis & Wills 1999), where He II $\lambda 1640$ and O III] $\lambda 1664$ were also excluded. The scatter is larger there, and the QSOs with the largest and smallest deviations from the fit are indeed the objects with smallest and largest weights in our SPC3 (§4.3, Table 1). This demonstrates that our SPC3, which involves the broad wings of the emission lines, is the major source of scatter in the Baldwin relationship. The remaining scatter of $\sim 10\%$ in our SPC1-derived Baldwin relationship is likely to result from non-linearity of the relationship(s), time variability of spectra, and inappropriateness of $L_{\nu}(1549)$ as a luminosity indicator. A bolometric or ionizing luminosity may be more appropriate. Even then, an apparent luminosity may not be that illuminating the emission-line gas.

Besides the strongest UV lines, which are already known to show a Baldwin effect from previous studies of direct measurements, such as Ly α , O I $\lambda 1304$, C IV $\lambda 1549$, He II $\lambda 1640$, C III] $\lambda 1909$, and Mg II $\lambda 2798$, SPC1 shows the Baldwin effect in other lines. N V $\lambda 1240$ appears in SPC1, showing that its equivalent width decreases with luminosity. This appears to conflict with some other studies (e.g., Espey & Andreadis 1999) that show no Baldwin effect for N V. This may be because, using direct spectral line measurements, N V is difficult to deblend from Ly α because of the uncertainties in line profiles and in determining the location of continuum in this region. N V and Ly α (and some other line blends) are easily resolved in our SPC1. Thus SPCA provides us with a valid way of disentangling the Baldwin effect for N V. We also find a Baldwin effect for Si IV+O IV] $\lambda 1400$. This has also been noted by e.g., Laor et al. (1995), Green, Forster, & Kuraszkiwicz (2001) although others claim no Baldwin effect for this feature (e.g., Cristiani & Vio 1990; FHFC; Osmer et al. 1994; Francis & Koratkar 1995).

Our broad UV-optical line coverage can also link Baldwin relationships for the UV lines with luminosity-dependent emission-line properties in the optical region. Our SPC1 shows that there is a Baldwin effect for the Balmer lines, and also for broad He II $\lambda 4686$. A Baldwin effect has been seen for H β by comparing

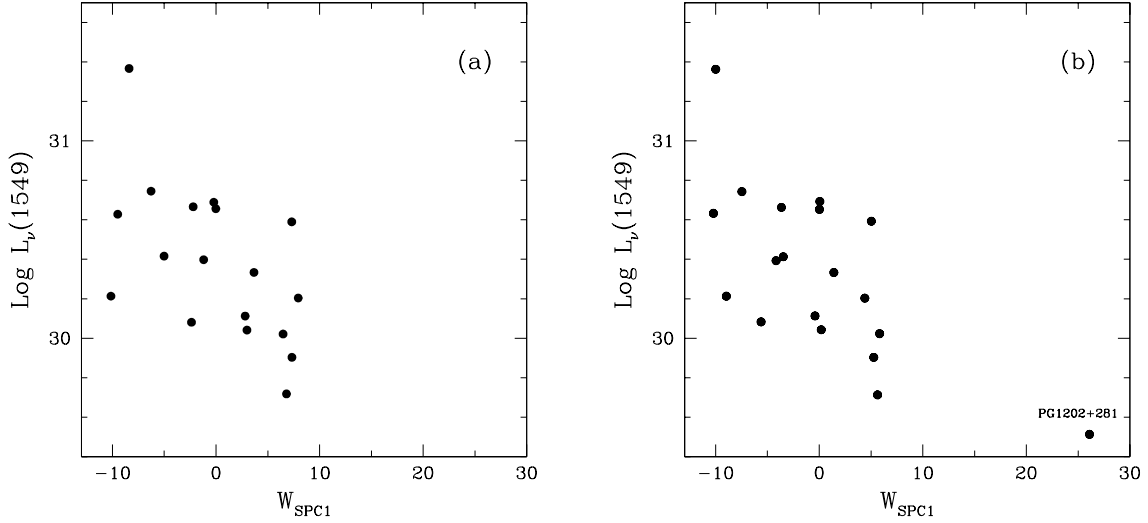


Fig. 5.— Continuum luminosity at C IV vs. weight of SPC1 (line-core component) from *separate* SPCA analyses (a) for 18 QSOs; (b) including PG 1202+281, the lowest luminosity QSO in our sample, included. Both correlations indicate a Baldwin Effect. The Pearson correlation coefficients are 0.58 and 0.69, and the two-tailed probability of these correlations arising by chance are 1.1% and 0.13%, respectively.

Table 4: Correlation Coefficients and Probabilities^a

| | W_{SPC1}^b | W_{SPC2}^b | W_{SPC3}^b | α_x^c | H β FWHM | $L_\nu(1549)$ | M_{BH} | L/L_{Edd} |
|--------------------|-------------------------|---------------------|--------------------------------------|--------------------------|----------------------|---------------|--------------------------|--------------------|
| W_{SPC1} | ... | ... | ... | ... | ... | ... | ... | ... |
| W_{SPC2} | 0 | ... | ... | ... | ... | ... | ... | ... |
| W_{SPC3} | 0 | 0 | ... | ... | ... | ... | ... | ... |
| α_x | -0.167 | +0.143 | -0.702^d (0.12%) | ... | ... | ... | ... | ... |
| H β FWHM | -0.112 | +0.101 | -0.838 ($<0.01\%$) | +0.731 (0.06%) | ... | ... | ... | ... |
| $L_\nu(1549)$ | -0.583 (1.1%) | -0.143 | -0.151 | +0.433 | +0.200 | ... | ... | ... |
| M_{BH} | -0.246 | +0.137 | -0.711 (0.09%) | +0.747 (0.04%) | +0.932 (0) | +0.335 | ... | ... |
| L/L_{Edd} | -0.024 | +0.002 | +0.722 (0.07%) | -0.499 (3.5%) | -0.909 (0) | +0.118 | -0.777 (0.01%) | ... |

^aThe table gives the Pearson correlation coefficients for an analysis of 18 QSOs and the two-tailed probability (in parenthesis) of that correlation arising by chance. Signs indicate a positive or negative correlation.

^bWeights of principal components for each QSO, for the SPCA of the Ly α to H α spectra of 18 QSOs.

^cSoft X-ray spectral index (L97).

^d3C 273 (PG 1226+023) has a significant radio-jet contribution to α_x and shows significant slope variations (L94). Excluding this QSO, the Pearson coefficient and probability are -0.894 and 10^{-6} .

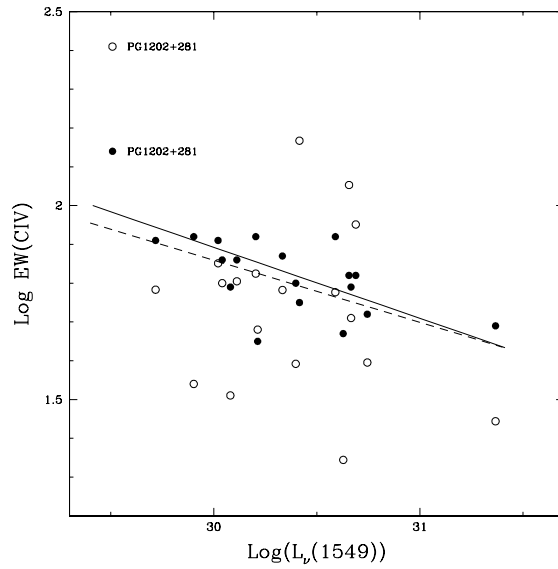


Fig. 6.— Baldwin Relationship for C IV. The filled circles represent EWs derived from SPC1 and the mean spectrum (§4.1). The solid line indicates the least-squares regression of the SPC1-derived EW on $\log L_\nu(1549)$. The open circles represent the integrated, direct, EW measurements from the original spectra (Francis & Wills 1999). The dashed line is the least-squares fit of the Baldwin relation from Kinney et al. (1990), showing the good agreement in both slope and normalization. (Note: PG 1202+281 is excluded from this SPCA analysis. Its SPC1 weight and therefore its derived EW in this plot, is estimated based on the tight relationship between the weight of the first principal component in this analysis and that in the analysis with PG 1202+281 included (Fig. 5a,b)).

the low and high redshift data of BG92 and McIntosh et al. (1999) (see Yuan et al. 2002), and an $H\beta$ Baldwin effect is included in the results of Espey & Andreadis (1999). However, Croom et al. (2002) find a positive correlation between $EW(H\beta)$ and luminosity. The reason why the Balmer-line Baldwin effect has been difficult to identify in the past, is probably because it has been masked, especially in integrated line measurements, by the scatter caused by BG PC1 in low redshift, optical samples. BG92 have shown an inverse luminosity dependence for the strength of broad $He II \lambda 4686$ (PC2 in their Table 2), and their Figs. 2 and 3 show how it has been masked by QSO-to-QSO differences in the strength of $Fe II(opt)$ emission.

It has been suggested that the slope of the Baldwin effect, β , is dependent on ionization (see Espey & Andreadis 1999; Croom et al. 2002). We can investigate the Baldwin effect for other broad emission lines besides C IV. We measure the equivalent widths of $Ly\alpha$, N V, C III]+Si III], Si IV+O IV] $\lambda 1400$, and Mg II the same way we do for C IV. We deblend $Ly\alpha+N V$ in the mean spectrum and measure the narrow components of $Ly\alpha$ and N V in SPC1. If indeed a linear approximation is valid when extracting the Baldwin effect from our SPC1, then the fractional change in integrated line equivalent width depends on the relative contributions from SPC1 and the mean spectrum. These relative contributions will determine the slopes that we find for the Baldwin effect. While β for C IV is uncertain to within ± 0.05 , the slopes for different emission lines relative to that for C IV can be determined quite accurately, depending only on the uncertainty in measuring the line strength in the mean spectrum. The weights, W_{SPC1} , are the same for each emission line. In Fig. 7 β is plotted against the ionization potential of each ion. The results are similar to the dependence shown in Espey & Andreadis’ Fig. 6. Except for N V, they suggest that their “slope of slopes” plot is consistent with predictions by Korista, Baldwin, & Ferland (1998) (also shown in their Fig. 6), based on a locally optimally emitting cloud distribution. Our N V is more consistent with these predictions.

In summary, our broad UV-optical line coverage links the luminosity-dependent BG PC2 with the Baldwin effect seen in large samples of UV spectra, covering a wide luminosity range. The arguments are as follows. Our SPC1 shows a dependence on luminosity, consistent with Baldwin relationships seen in these larger samples. The line cores of our SPC1 are like those seen in the FHFC UV SPC1, for which FHFC, and Francis & Koratkar (1995) have clearly demonstrated a Baldwin effect. Our SPC1 extends to the optical, showing a luminosity dependence for the Balmer lines and the broad $He II \lambda 4686$. BG92’s luminosity eigenvector, BG PC2, involves the Balmer line equivalent widths and broad $He II \lambda 4686$ (B02). We therefore identify BG PC2 with our SPC1, and conclude that the BG PC2 is effectively the optical part of Baldwin relationships derived from UV spectra. Table 5 lists the identifications of the principal components and correlated external parameters.

Table 5: Identifications of the principal components and key external parameters*

| Component | Related parameters |
|-----------------------|---|
| SPC1, line-core | SPC2 in Fig 2, BG PC2, FHFC SPC1, Baldwin effect, $L_\nu(1549)$ |
| SPC2, continuum slope | FHFC SPC2 |
| SPC3, line-width | SPC1 in Fig 2, BG PC1, α_x |

*See Table 4 for correlations.

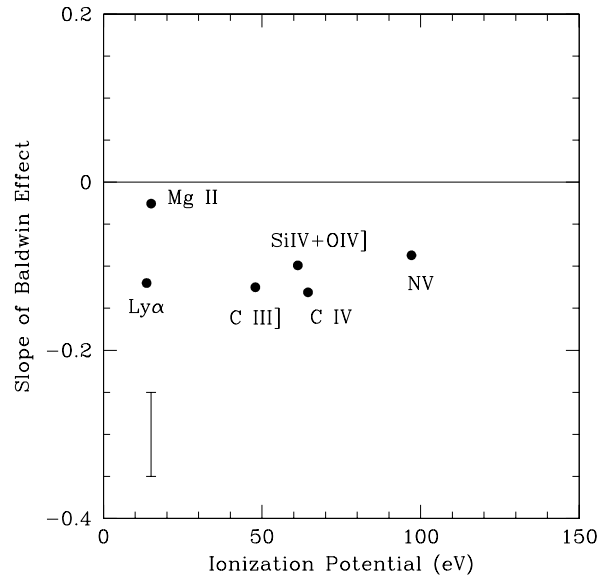


Fig. 7.— Ionization dependence of Baldwin relationships. The slope of the Baldwin relationship for each line is plotted against the ionization potential of the ion responsible (or mean potential in the case of Si IV+O IV] λ 1400). The error bar indicates the uncertainty for C IV from the least-squares fitting. The relative uncertainties from line-to-line are much smaller and depend on the accuracy of the EW denominator – the integrated line measurement in the mean spectrum.

4.2. The Second Principal Component: Continuum Slope

Our second principal component (Fig. 3, SPC2) is almost a pure continuum component. It shows a slope at wavelengths less than $\sim 4000 \text{ \AA}$ but flattens out in the optical region. This seems to be consistent with the continuum slope reported by FHFC in the LBQS sample, but covers a much broader wavelength range. The line features in this component are relatively weak, if not absent, and probably arise from crosstalk from the other components (see §4.5). The continuum slope has a factor of 6 greater variation in this component than in the line-core component and, therefore, accounts for most of the continuum slope variation in the sample. The SPC2 weights, hence continuum slopes, are independent of luminosity (Table 4).

The continuum slope variation could be the result of an intrinsic variation in the QSO continuum, e.g., the big blue bump, differing amounts of starlight from the host galaxy, or different amounts of reddening by dust associated with the QSO. Any one of these possible contributions could be orientation dependent. We have not yet corrected our spectra for known contributions from the host galaxy, and this is significant at longer wavelengths for a few of the QSOs. It is likely that dust absorption plays an important role, as we find a correlation between optical-UV continuum reddening, intrinsic UV absorption lines, and flatter soft X-ray slope (Wills, Shang, & Yuan 2000; Brandt, Laor, & Wills 2000). If dust were the main factor producing the continuum slope variation, we can expect it to be external to the BLR because it would obscure the line and continuum emission equally and hence leave the equivalent width unchanged — a featureless principal component, as seen.

4.3. The Third Principal Component: Line-width Relationships

The $H\beta - [O\text{III}]$ region of the third principal component (SPC3 in Fig. 3) in our analysis of the entire UV-optical spectrum is very similar to that of the SPCA of the $H\beta - [O\text{III}]$ region alone (SPC1 in Fig. 2). Fig. 8 compares the weights of the two principal components and shows quantitatively that these components are closely related. In SPC3, there is a clear anticorrelation between the strengths of $[O\text{III}]$ and $\text{Fe II}(\text{opt})$ emission and between $H\beta$ width and the strength of $\text{Fe II}(\text{opt})$. Therefore, BG PC1 relationships are an important part of the third principal component in our analysis of the UV-optical spectrum. A prominent feature is the correlated line widths of the low ionization broad emission lines – $H\beta$, Mg II and $H\alpha$ (the “W” shape, see §4.5). Deblending of the $\lambda 1909$ feature in this sample shows that the width of $\text{C III}]$ also varies like $H\beta$ (Wills, Shang, & Yuan 2000). Important variables in the BG PC1 eigenvector are $\text{FWHM}(H\beta)$ and the soft X-ray spectral index α_x (BG92, L94, L97). Our W_{SPC3} is directly correlated with $\text{FWHM}(H\beta)$ and also with α_x (Fig. 9a, b, Table 4).

The SPC3 C IV feature extends over more than 30000 km s^{-1} . $\text{C IV } \lambda 1549$ does not show an obvious correlated line-width change in SPC3. The characteristic “W” shape may not appear, though, if the line strength increases with line width. For integrated line measurements it is also the case that $\text{FWHM}(\text{C IV})$ does not correlate well with the widths of the low-ionization lines in this sample (Fig. 4 of Wills et al. 2000), but in these cases, the SPC1 line core contributes some scatter to the direct measurements of $\text{FWHM}(\text{C IV})$ (contributing to the inverse correlation between $\text{EW}(\text{C IV})$ and $\text{FWHM}(\text{C IV})$, Brotherton et al 1994b, §5).

As expected, the $\text{Fe II}(\text{opt})$ features centered near 4570 \AA and 5250 \AA are positively correlated with Fe II optical multiplets 27 and 28, prominent features measured at 4178 \AA , 4237 \AA , and 4308 \AA (Phillips 1977, 1978). Along with increasing strength of $\text{Fe II}(\text{opt})$, several low-ionization lines increase in strength: $\text{Si II } \lambda 1263$, $\text{O I } \lambda 1304$, $\text{C II } \lambda 1335$, $\text{N III } \lambda 1750$, and probably $\text{Na I } \lambda 5892$ (for the last, see Thompson 1991). $\text{Si IV} + \text{O IV } \lambda 1400$ is also positively correlated with $\text{Fe II}(\text{opt})$. The strengths of the prominent broad emission

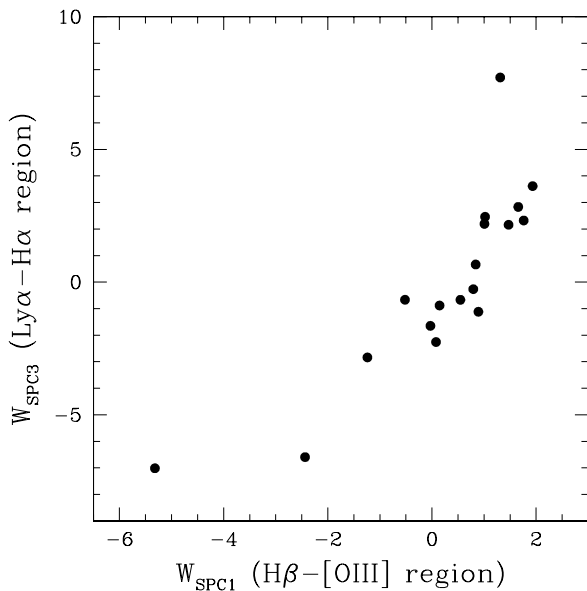


Fig. 8.— W_{SPC3} for the $\text{Ly}\alpha - \text{H}\alpha$ region vs. W_{SPC1} for the $\text{H}\beta - [\text{O III}]$ region. The W_{SPC3} are from the SPCA of the UV-optical spectra of 18 QSOs illustrated in Fig. 3. The W_{SPC1} are for 18 QSOs of the SPCA of 22 QSO spectra of the $\text{H}\beta - [\text{O III}]$ region illustrated in Fig. 2. It shows that the two principal components from the two separate SPCA are closely related.

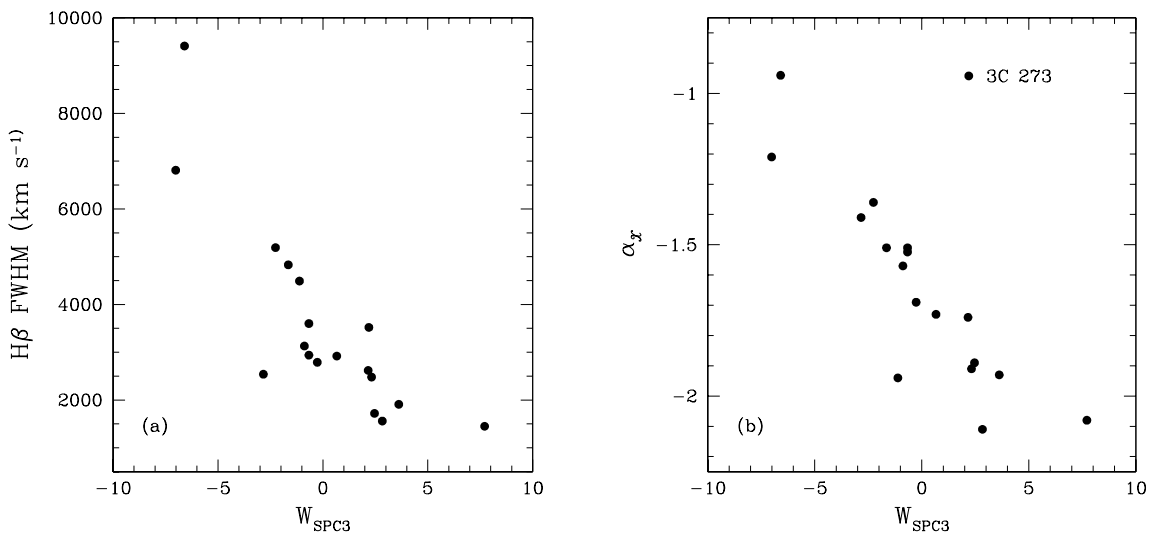


Fig. 9.— $\text{H}\beta$ FWHM and α_x vs. W_{SPC3} from the SPCA of the UV-optical spectra of 18 QSOs. Note that the soft X-ray spectrum of 3C 273 has a significant jet contribution, and is time variable (L94).

lines correlate together – $\text{Ly}\alpha$, C IV , Mg II , $\text{H}\beta$, & $\text{H}\alpha$, but are anticorrelated with the low ionization lines mentioned above.

Another important new result revealed by SPC3 is the strong anticorrelation between broad UV Fe II emission blends (the small blue bump) and the optical Fe II blends. This was actually predicted by Netzer & Wills (1983). They showed that strong Fe II(opt) requires high optical depth in the UV resonance transitions of Fe II. At the same time, these high optical depths result in destruction of UV Fe II photons, in particular, by ionization from the $n=2$ level of H I (Balmer continuum). Green (1998) found from composite spectra of samples of steep and flat optical-X-ray spectral index, α_{ox} , that UV and optical Fe II emission are correlated in opposite senses with α_{ox} . This suggests the anti-correlation between UV and optical Fe II blends found here.

SPC3 reveals most of the UV-optical BGP C1 relationships demonstrated by direct emission-line and continuum measurements (Wills et al. 1999a). A descriptive summary of the relationships among UV-optical parameters in SPC3 is shown in Fig. 10, which is related to Fig. 4 in Wills et al. (1999b). This component has a flat continuum (SPC3 in Fig. 3), so changes in UV-optical continuum shape are not obviously related to the SPC3 correlations.

4.4. Exclusion of absorption-line QSOs and PG1202+281

Four QSOs were excluded from the above analysis: PG 1202+281, because of its extremely large equivalent widths, and the three strong absorption-line QSOs (PG 1001+054, PG 1114+445 and PG 1411+442), because their $\text{Ly}\alpha$ and C IV absorption features occur at different outflow velocities and thus introduce spurious features in the principal component spectra.

To investigate the effect of the absorption-line QSOs, we have repeated the SPCA both excluding the affected wavelengths, and interpolating over the absorption features. The results are essentially unchanged from those discussed above.

Including PG 1202+281, with or without the three absorption-line QSOs, does not substantially change the results (see Fig. 5, Fig. 8). This is seen by comparing the SPCA for the whole sample of 22 QSOs (Fig. 11) with the adopted SPCA in Fig. 3. Because of its extreme properties, PG 1202+281 causes a significant rotation of the principal component axes, so the results of Fig. 11 should be viewed with caution. The resulting crosstalk probably accounts for the relatively strong [O III] emission in the SPC1 spectrum of Fig. 11. While PG 1202+281 seems to be consistent with the same principal components relationships as the other QSOs (see Fig. 5), its differences may hint at additional physical processes, or extend our parameter space to a non-linear regime. Either way, this is a limitation of our small sample size; a large sample covering a wider range of parameter space is needed to address these possibilities. In order not to give PG 1202+281 undue weight in the analysis, we could have carried out SPCA using the ranks of fluxes in each wavelength bin or using logarithmic flux scales. For simplicity and directness of interpretation, we have chosen not to transform the flux densities. Therefore we have excluded PG 1202+281.

4.5. Simulations

The principal components arising from PCA can be directly interpreted only if the input parameters (i.e. the fluxes in all the bins in this study) are related linearly. In our SPCA, variable line width will usually

introduce non-linear relationships among the affected binned flux densities, i.e., the flux densities do not change linearly in different bins when the line width changes. As an aid to interpretation we have therefore made simulations with artificial data (see also Mittaz, Penston, & Snijders 1990). Fig. 12 shows an example in which we apply SPCA to 40 spectra with added Poisson noise. Each spectrum has 7 line features and a continuum slope, with possible relationships as indicated by the real data. Lines 1, 2 and 3 have one narrow and one broad Gaussian component. Three independent sets of relationships among lines and continuum are included in the spectra:

1. The narrow components of lines 1, 2 and 3 have a fixed width; their strengths vary in proportion to each other.
2. The broad components of lines 1, 2 and 3 have a fixed strength, but their widths are proportional to the strength of lines 4 and 5. The strengths of lines 4 and 5 are also proportional, and they are inversely proportional to the strengths of lines 6 and 7.
3. Each spectrum has a different linear continuum slope, which is not related to any line feature.

The simulation results clearly show that:

1. The three sets of relationships are separated into the three principal components in the order expected.
2. There is crosstalk among the three principal components, which is caused by the non-linear effect of line width change and the continuum slope (see §5), for example, lines 1, 2 and 5 in principal component 3 (the slope), and line 5 in principal component 1. (The change in continuum level changes the line equivalent widths. But this is a real, linear effect, and not crosstalk.)
3. The line width change produces a “W” shape in the principal component (or an “M” shape if the y axis flips), as can be seen in principal component 2 for the broad components of lines 1, 2, and 3. This can be visualized as the changes in the line wings.

These simulation results show that SPCA is able to successfully distinguish the relationships that we input.

Is our interpretation really unique? Could a non-linear relationship produce two principal components like our SPC1 (line-core) and SPC3 (line-width)? In order to test this, we did a simulation with three Lorentzian line profiles for which $\text{FWHM} \propto 1/I_p - c$, where I_p is the peak flux of the lines, c is a constant chosen to vary FWHM by a factor of 6, while I_p varies by a factor of 3. These ranges reproduce differences seen in our real spectra. The results of SPCA are shown in Fig. 13. The standard deviation spectrum shows a peak on a broad base, somewhat similar to $\text{H}\beta$, $\text{H}\alpha$, and CIV in our real data. In the simulated SPC1, weak line wings anticorrelate with a line core. This is the major part of the relationship we input, and is produced by the Lorentzian’s sharp peak and very broad wings. This is qualitatively seen in the real SPC1 for $\text{H}\alpha$, CIV , and possibly $\text{H}\beta$. In the simulated SPC2 we see the “W” signature resulting from crosstalk caused by the non-linearity introduced by changes in line-width. As expected, SPC1 accounts for much more intrinsic variance than the “crosstalk” component, SPC2.

To summarize, this Lorentzian simulation shows that, mathematically, correlated line-width changes of profiles with a sharp peak and broad wings could produce two principal components similar to SPC1 and SPC3 seen in our analysis of real data. Nevertheless, the conclusions derived from the real data would not be

changed much: The emission from low velocity gas depends on luminosity, a completely independent external parameter, but emission from non-line-core gas does not – the Baldwin Effect remains. SPC3 weights clearly correlate with directly measured $\text{FWHM}(\text{H}\beta)$, and with the completely independent external parameter, α_x . A simple Lorentzian model does not account for the correlations with external parameters; nor does it account for the different line ratio in observational principal components.

5. DISCUSSION

Over the spectral range from $\text{Ly}\alpha$ to $\text{H}\alpha$, SPCA shows that 78% of the intrinsic spectrum-to-spectrum variance is accounted for by just three principal components (Table 2). In Table 2 we also compare the fractional contributions to the total intrinsic variance within the UV and near-UV–optical wavelength ranges. We find that SPC1 contributes about half the variance in the UV, similar to the FHFC result for 232 LBQS UV spectra. Examination of SPC3 and higher-order component spectra, and comparison with simulations, clearly shows the non-linear contributions of spectrum-to-spectrum line-profile differences, for example, differences caused by changing width, probably kurtosis and asymmetry as well (see for example, FHFC). We therefore tabulate the sum of the variances from SPC3 through SPC10 (noise increasingly dominates higher order principal components), as probably representative of the line-width component. In the UV, the line-core component clearly dominates. In the 2100 Å – 6607 Å range, the line-width relationships clearly dominate the line-core component and have a contribution similar to that from the continuum principal component. The increasing dominance of the line-width relationships is not surprising given the previous results from SPCA (Fig. 2 and BG92). It is easy to understand why historically the $\text{Fe II}-[\text{O III}]-\text{H}\beta$ -width correlations were discovered for low-redshift QSOs in the optical region, and the Baldwin effect in the UV spectra of high-redshift QSOs. The line-core, line-width and continuum sets of relationships together appear to account for about 78%–95% of the spectrum-to-spectrum intrinsic variance.

Much of the remaining intrinsic variance is likely to arise from departures from linearity – among the Baldwin and line-width relationships for different emission lines, in the description of the continuum-to-continuum differences – and from time-variability. Pogge & Peterson (1992) showed that, for Seyfert galaxies, there is a relationship between line and continuum luminosity, as an individual Seyfert nucleus varies in time. For example, for $\text{C IV } \lambda 1549$, they showed $\text{EW}(\text{C IV}) \propto L^{-0.72}$, with a slope different from that for the global (QSO-to-QSO) relationship with exponent of -0.17 (§4.1, Peterson 1997). They suggested that this intrinsic “Baldwin relationship” accounts for the scatter seen in the global relationship. They also demonstrated that additional scatter is introduced by the the lag of emission-line response to continuum variations. We estimate the lag to contribute typically $<5\%$ to the variations in EW in our data (Fig. 6) judging from the $\text{H}\beta$ lags and light curves presented by Kaspi et al. (2000) and Giveon et al. (1999). If the mechanism underlying the intrinsic Baldwin Effect is similar to that underlying the global Baldwin Effect, this source of scatter may be included in our SPC1 or SPC3 components. If the intrinsic and global Baldwin Effects are independent, then the intrinsic Baldwin Effect will contribute to the residual $\sim 5\%$ variance, but not to the relationships represented by the line-core and line-width components. That is, this source of variance would not be important in Fig. 5.

5.1. The Physics Behind the Line-core and Line-width Components

The simulation with Lorentzian line profiles (§4.5, Fig. 13) shows that SPCA could mathematically produce a line-core and a line-width component from a non-linear relationship. One may argue that the results from the real QSO spectra suffer from the same problem. However, the correlations shown in Table 4 and in Figs. 5 and 9b show that the components derived from the real spectra are physically meaningful based on their distinct correlations with the external variables α_x and L . In §4.1 we have presented additional arguments that the line-core component represents the Baldwin relationship and is dependent on luminosity (possibly related to accretion rate, \dot{M}). Our small sample, with a limited range in L , does not allow us to distinguish whether the line-width components are related to black hole mass, $M_{\text{BH}} \propto \text{FWHM}(\text{H}\beta)^2 L^{1/2}$, or to Eddington accretion ratio, $L/L_{\text{Edd}} \propto L/M_{\text{BH}} \propto \text{FWHM}(\text{H}\beta)^{-2} L^{1/2}$ (Table 4). However, the dependence of the SPC3 weights on α_x , suggests, by analogy with Galactic black-hole candidates, that this component is driven by Eddington accretion ratio (L94, L97, Yuan et al. 2002). Stronger EW Fe II(opt), Fe II(opt)/Fe II(UV), and the Fe II(opt) – [O III] anticorrelation indicate that more dense gas is available to fuel the central engine. Stronger Fe II(opt) is associated with narrower FWHM(H β), consistent with an Eddington ratio interpretation of SPC3. Further support for a physical difference between SPC1 and SPC3 gas is indicated by line-intensity ratios: Brotherton et al. (1994a) showed that the emission-line ratios for gas of low- and high-velocity dispersion indicate different photoionizing flux, ionization state, and density.

The near-absence of emission in SPC1 from gas with high-velocity dispersion, and the luminosity independence of SPC3, suggest that the line emission represented by SPC3 has EW \sim constant. Could the global Baldwin relationship be explained by a very simple model in which a total line equivalent width is the sum of the equivalent width of the line-width component (\sim constant), and that of the line-core component ($\propto L_{\text{cont}}^{-1}$), i.e., $\text{EW}(\text{total}) = a + bL_{\text{cont}}^{-1}$? Such a dependence can fit our own data, but cannot fit the Baldwin effect data for large samples, such as that of Kinney et al. (1990), covering seven orders of magnitude in luminosity.

5.2. Separating the Line-core and Line-width Spectra

Since the relationships represented by the line-core and line-width spectral principal components have real, independent, physical origins, it would be appropriate to model these relationships independently rather than, as in the past, trying to model the observed integrated equivalent widths (e.g., Korista et al. 1998; Kuraszek et al. 2000). A case in point may be attempts to ascribe an ionization-potential dependence to β , the exponent of the Baldwin relationship. The *relative* values of β are quite accurately determined for different emission lines, but the scatter is large (Fig. 7). The large scatter may be attributed to the use of integrated EWs with a significant contribution from non-core emission because the non-core line ratios are independent of those in SPC1 gas.

One possibility is to perform a SPCA on a sample of simulated model spectra, making a comparison of the resulting SPC spectra with those from a SPCA of the observed spectra. Another approach might be to use the principal component spectra to derive separate spectra for the (assumed separate) gas components responsible for the line-core and line-width components, and compare each of these with photoionization models. This was attempted by Brotherton et al. (1994a) who decomposed UV emission lines into components representing intermediate and very broad line regions (ILR and VBLR). Our SPCA shows that their VBLR is an over-simplification. While their ILR is similar to our SPC1 component, we do not define a VBLR, but rather a line-width component (dominated by our SPC3), where line widths range from the narrowest

to broadest $H\beta$ lines observed (FWHM from 1500 to 9500 km s⁻¹). Thus the ILR derived by Brotherton et al. (1994a) would include SPC1 emission as well as low-velocity emission from the line-width component. However, the technique of best-fitting a combination of line-core and line-width spectra still seems promising. Further discussion is beyond the scope of the present paper.

While the ILR has been directly related to the Baldwin effect (Brotherton et al. 1994a, FHFC, Francis & Koratkar 1995), the relationship of the UV ILR to the optical BG PC1 has been controversial, including the question of whether BG PC1 is part of the Baldwin relationship, or whether it is the cause of its enormous scatter (Brotherton & Francis 1999). Because of our wide wavelength coverage we have been able to demonstrate clearly that these two sets of relationships are orthogonal. Brotherton & Francis (1999) came to a different conclusion, based on their finding of increasing ILR strength with [O III] λ 5007, a strong SPC3 or BG PC1 parameter. This may be because of the ILR decomposition problem mentioned above.

6. SUMMARY AND CONCLUSIONS

Our Spectral Principal Component Analysis of an essentially complete sample of 22 PG QSOs yielded three significant linear spectral principal components accounting for $\sim 78\%$ of the intrinsic variance among emission-line and continuum spectra over the wavelength range from Ly α to H α (excluding the three QSOs with strong intrinsic absorption and the extreme object PG1202+281). Spectral Principal Component 1 dominates the UV emission lines, accounts for $\sim 41\%$ of the intrinsic spectrum-to-spectrum variance, and is identified with the Baldwin relationships. Spectral Principal Component 2 accounts for most of the continuum variations, contributing $\sim 23\%$ of the total intrinsic variance. Spectral Principal Component 3 is directly related to the first Principal Component in the PCA of integrated line measurements in the Fe II–H β –[O III] region by BG92. It includes line-width, which introduces non-linear relationships among flux bins across emission lines, and therefore propagates to higher-order Principal Components in our linear analysis. This line-width component dominates the Fe II–H β –[O III] region, and accounts for between 14% and 31% of the sample’s total intrinsic variance. Tables 2 and 5 summarize these results.

6.1. The Baldwin Effect and SPC1

1. SPC1 is dominated by emission from gas of low velocity dispersion (FWHM 2000 – 3000 km s⁻¹), but also includes broad He II λ 4686 (FWHM 4880 km s⁻¹).
2. The weights of this principal component correlate with the QSOs’ luminosities.
3. Deriving the equivalent widths from this principal component leads to a Baldwin relationship in good agreement with the slope and normalization determined for much larger samples and luminosity ranges spanning 7 orders of magnitude.
4. The narrow (FWHM 2000 – 3000 km s⁻¹) features in our Spectral Principal Component 1 agree in profile and line intensity ratios with those derived from SPCA for much larger LBQS samples using just UV spectra from Ly α to the C III] blend (Principal Component 1, from Francis et al. 1992; Francis & Koratkar 1995), and inferred by comparison of mean UV spectra of low and high luminosity QSOs (Osmer et al. 1994), and of low and high X-ray brightness QSOs divided by α_{ox} (Green 1998). Francis & Koratkar (1995) showed quantitative agreement with the Baldwin effect, for their large, but low signal-to-noise ratio sample.

5. The strong, broad He II $\lambda 4686$ links our SPC1 directly with the “luminosity” principal component derived by BG92 and B02 from direct measurements.
6. The Baldwin relation determined from direct equivalent width measurements would not be expected to be very significant for a sample the size of ours and covering only 2 orders of magnitude in luminosity. However we demonstrate a significant reduction in scatter using SPCA-derived EWs, over those measured directly. The line-width components contribute most of the scatter in the Baldwin relationships. This demonstrates the potential of SPCA-derived EWs to define a much cleaner Baldwin relation for future investigations of emission line response to the ionizing continuum, perhaps with applications to cosmology (relations between luminosity distance and redshift).
7. We have determined the Baldwin relationships for different emission lines, confirming that the effect is present for the Balmer lines. UV and optical Fe II emission-line blends are very weak or absent from our “Baldwin Effect” principal component.
8. Our clean separation of Ly α and N V in SPC1 shows a significant Baldwin effect for N V. This result is in striking contrast with the slope derived from direct measurements, where the EW shows a positive slope (increases) with luminosity.

6.2. The Line-width Components (SPC3 and higher order)

1. We have demonstrated clearly that the third principal component is directly related to BG92’s first principal component. The SPC3 weights are shown to directly correlate with FWHM($H\beta$) and with α_x , parameters that are important in BG PC1 correlations in the $H\beta$ region (BG92 and L94, L97).
2. We present a number of emission line correlations, both positive and negative. Of particular note is a clear anticorrelation between optical and UV Fe II blends, as predicted by Netzer & Wills (1983).
3. Laor (1998), and Gebhardt et al. (2000) have demonstrated a calibration of black hole mass in terms of FWHM $H\beta$ and luminosity, as if $H\beta$ line width is determined by virial motions. The line-width correlations demonstrated by this component, between Balmer lines and Mg II, and FWHM C III] has also been shown to correlate with $H\beta$ (Wills et al. 1999), suggesting that this calibration can be used to investigate black-hole mass relationships at higher redshifts ($z \gtrsim 2 - 3.5$), where Mg II and C III] are accessible to ground-based spectroscopy (see also McLure & Jarvis 2002).

6.3. The Relation Between Line-width and Line-core Components

We have demonstrated the power of our wide wavelength coverage combined with SPCA to link two independently-discovered luminosity relationships at high and low redshift, showing that the BG92 and B02 luminosity principal component of low redshift samples is directly related to the Baldwin effect in higher redshift, UV spectra, and showing that BG PC1 (or the line-width principal component) relationships are the cause of enormous scatter in Baldwin relationships derived from integrated, direct, EW measurements. We show how Baldwin relationships can be derived using SPCA, virtually eliminating the scatter. Such spectrum-luminosity relationships might be used to determine z -independent luminosities, hence to derive L - z relationship at high z . This rekindles the hope that Baldwin relationships can be used for cosmology. The line-width principal components are related to black-hole mass or Eddington accretion ratio, and their

clean separation from the Baldwin relationships can, in principle, lead to their use to trace QSO evolution. The wide wavelength coverage and SPCA also provides a strong visual impressions of spectral relationships that provide a guide for future direct line measurements and analysis.

We thank Paul Francis and Mike Brotherton for many discussions, and for comments on a draft of this paper. We appreciate Bill Jefferys' help with the Bayesian analysis, and thank Scott Croom for a copy of his paper in advance of publication. We also thank the referee, Paul Green, for his valuable suggestions and careful reading of the paper. We gratefully acknowledge the help of C. D. (Tony) Keyes and A. Roman of STScI, M. Dahlem (now of ESTEC), David R. Doss, Jerry Martin, Earl Green, and Larry Crook at McDonald Observatory, and also M. Cornell and R. Wilhelm, who provided computer support in the Astronomy Department, and at McDonald. BJW acknowledges financial support by NASA through LTSA grant NAG5-3431 and grant GO-06781 from the Space Telescope Science Institute which is operated by the Association of Universities for Research in Astronomy, Inc., under NASA contract NAS5-26555. We have made use of the NASA/IPAC Extragalactic Database (NED), which is operated by the Jet Propulsion Laboratory, California Institute of Technology, under contract with NASA.

REFERENCES

- Alexander, T., & Netzer, H. 1994, *MNRAS*, 270, 781
- Baldwin, J. A. 1977, *ApJ*, 214, 679
- Baldwin, J. A., Wampler, E. J., & Gaskell, C. M. 1989, *ApJ*, 338, 630
- Baldwin, J. A., Ferland, G., Korista, K., & Verner, D. 1995 *ApJ*, 455, L119
- Bohlin, R. C. 1996, *AJ*, 111, 1743
- Bohlin, R. C. 2000, *AJ*, 120, 437
- Boroson, T., & Green, R. F. 1992, *ApJS*, 80, 109 (BG92)
- Boroson, T. A. 2002, *ApJ*, 565, 78 (B02)
- Bottoff, M. C., & Ferland, G. J. 2001, *ApJ*, 549, 118
- Brandt, W. N., Laor, A., & Wills, B. J. 2000, *ApJ*, 528, 637
- Brotherton, M. S., Wills, B. J., Francis, P. J., & Steidel, C. S. 1994a, *ApJ*, 430, 495
- Brotherton, M. S., Wills, B. J., Steidel, C. C., & Sargent, W. L. W. 1994b, *ApJ*, 423, 131
- Brotherton, M. S., & Francis, P. J. 1999, in *ASP Conf. Series 162, Quasars and Cosmology*, ed. G. J. Ferland, & J. A. Baldwin (San Francisco: ASP), 395
- Cristiani, S., & Vio, R. 1990, *A&A*, 227, 385
- Croom, S. M. et al. 2002, *MNRAS*, 337, 275
- Espey, B. R., & Andreadis, S. 1999, in *ASP Conf. Series 162, Quasars and Cosmology*, ed. G. J. Ferland, & J. A. Baldwin (San Francisco: ASP), 351

- Fabian, A. C. 1999, MNRAS, 308, L39
- Ferrarese, L., & Merritt, D. 2000, ApJ, 539, L9
- Ferland, G. J., & Baldwin, J. A. 1999, ASP Conf. Series 162, Quasars and Cosmology (San Francisco: ASP)
- Francis, P. J., Hewett, P. C., Foltz, C. B., & Chaffee, F. H. 1992, ApJ, 398, 476 (FHFC)
- Francis, P. J., & Wills, B. J. 1999, in ASP Conf. Series 162, Quasars and Cosmology, ed. G. J. Ferland, & J. A. Baldwin (San Francisco: ASP), 373
- Francis, P. J., & Koratkar, A. 1995, MNRAS, 274, 504
- Gebhardt, K. et al. 2000, ApJ, 543, L5
- Gilli, R., Salvati, M., & Hasinger, G. 2001, A&A, 366, 407
- Giveon, U., Maoz, D., Kaspi, S., Netzer, H., & Smith, P. S. 1999, MNRAS, 306, 637
- Goldschmidt, P., Miller, L., La Franca, F., & Cristiani, S. 1992, MNRAS, 256, 65
- Green, P. J. 1998, ApJ, 498, 170
- Green, P. J., Forster, K., & Kuraszkiewicz, J. 2001, ApJ, 556, 727
- Kaspi, S., Smith, P. S., Netzer, H., Maoz, D., Jannuzi, B. T., & Giveon, U. 2000, ApJ, 533, 631
- Kinney, A. L., Rivolo, A. R., & Koratkar, A. P. 1990, ApJ, 357, 338
- Korista, K. T., Baldwin, J. A., & Ferland, G. J. 1998, ApJ, 507, 24
- Korista, K. T. 1999, in ASP Conf. Series 162, Quasars and Cosmology, ed. G. J. Ferland, & J. A. Baldwin (San Francisco: ASP), 429
- Kormendy, J., & Ho, L. C. 2000, to appear in The Encyclopedia of Astronomy and Astrophysics (Institute of Physics Publishing), astro-ph/0003268
- Kuraszkiewicz, J., Wilkes, B. J., Czerny, B., & Mathur, S. 2000, ApJ, 542, 692
- Laor, A., Fiore, F., Elvis, M., Wilkes, B. J., & McDowell, J. C. 1994, ApJ, 435, 611 (L94)
- Laor, A., Bahcall, J. N., Jannuzi, B. T., Schneider, D. P., & Green, R. F. 1995, ApJS, 99, 1
- Laor, A., Fiore, F., Elvis, M., Wilkes, B. J., & McDowell, J. C. 1997, ApJ, 477, 93 (L97)
- Laor, A. 1998, ApJ, 505, L83
- Marconi, A., & Salvati, M. 2002, in ASP Conf. Proc. 258, Issues in Unification of AGNs, ed. R. Maiolino, A. Marconi, & N. Nagar (San Francisco: ASP), 217
- McIntosh, D. H., Rieke, M. J., Rix, H.-W., Foltz, C. B., & Weymann, R. J. 1999, ApJ, 514, 40
- McLure, R. J., & Jarvis, M. J. 2002, MNRAS, 337, 109
- Mickaelian, A. M., Gonçalves, A. C., Véron-Cetty, M. P., & Véron, P. 2001, Astrophysics, 44, 14
- Mittaz, J. P. D., Penston, M. V., & Snijders, M. A. J. 1990, MNRAS, 242, 370

- Murray, N., & Chiang, J. 1997, *ApJ*, 474, 91
- Netzer, H., & Wills, B. J. 1983, *ApJ*, 275, 445
- Netzer, H., & Peterson, B. M. 1997, in *Astronomical Time Series*, ed. D. Maoz, A. Sternberg, & E. Leibowitz (Dordrecht: Kluwer), 85
- Osmer, P. S., Porter, A. C., & Green, R. R. 1994, *ApJ*, 436, 678
- Peterson, B. M. 1997, *An Introduction to Active Galactic Nuclei*, p91 (United Kingdom:Cambridge University Press)
- Phillips, M. M. 1977, *ApJ*, 215, 746
- Phillips, M. M. 1978, *ApJ*, 226, 736
- Pogge, R. W., & Peterson, B. M. 1992, *AJ*, 103, 1084
- Pounds, K. A., Done, C., & Osborne, J. P. 1995, *MNRAS*, 277, L5
- Predehl, P., & Schmitt, J. H. M. M. 1995, *A&A*, 293, 889
- Schmidt, M., & Green, R. F. 1983, *ApJ*, 269, 352
- Scoville, N., & Norman, C. *ApJ*, 332, 163
- Silk, J., & Rees, M. J. 1998, *A&A*, 331, L1
- Thompson, K. L. 1991, *ApJ*, 374, 496
- Wampler, E. J. & Ponz, D. 1985, *ApJ*, 298, 448
- Wandel, A., Peterson, B. M., & Malkan, M. A. 1999, *ApJ*, 526, 579
- Wills, B. J., Laor, A., Brotherton, M. S., Wills, D., Ferland, G. J., & Shang, Zhaohui 1999a, *ApJ*, 515, L53
- Wills, B. J., Brotherton, M. S., Laor, A., Wills, D., Wilkes, B. J., Ferland, G. J., & Shang, Zhaohui 1999b, in *ASP Conf. Series 162, Quasars and Cosmology*, ed. G. J. Ferland, & J. A. Baldwin (San Francisco: ASP), 373
- Wills, B. J., Brotherton, M. S., Laor, A., Wills, D., Wilkes, B. J., & Ferland, G. J. 1999c, in *ASP Conf. Ser. 175, Structure and Kinematics of Quasar Broad Line Regions*, ed. C. M. Gaskell, W. N. Brandt, M. Dietrich, D. Dultzin-Hacyan, & M. Eracleous (San Francisco: ASP), 241
- Wills, B. J., Shang, Zhaohui, & Yuan, Juntao 2000, *New Astronomy Reviews*, 44, 511
- Yuan, Juntao, & Wills, B. J. 2002, in preparation

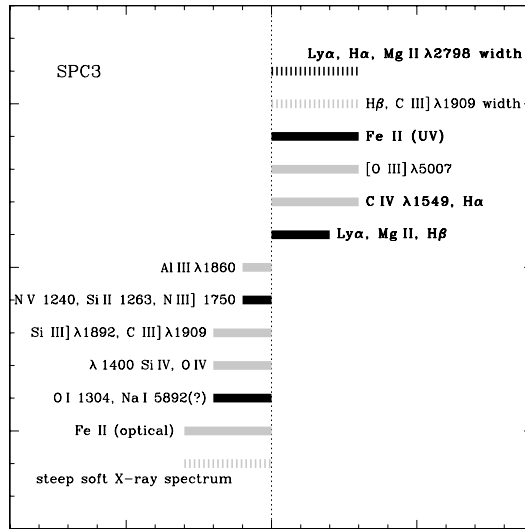


Fig. 10.— A descriptive summary of correlations related to the line-width component. Variables on the same side correlate positively with each other, and on opposite sides, negatively. Black bars show new correlations found in this study. Solid bars are for line strengths, and dotted bars are for line width and other parameters. The lengths of the bars indicate qualitatively the strength of the correlation.

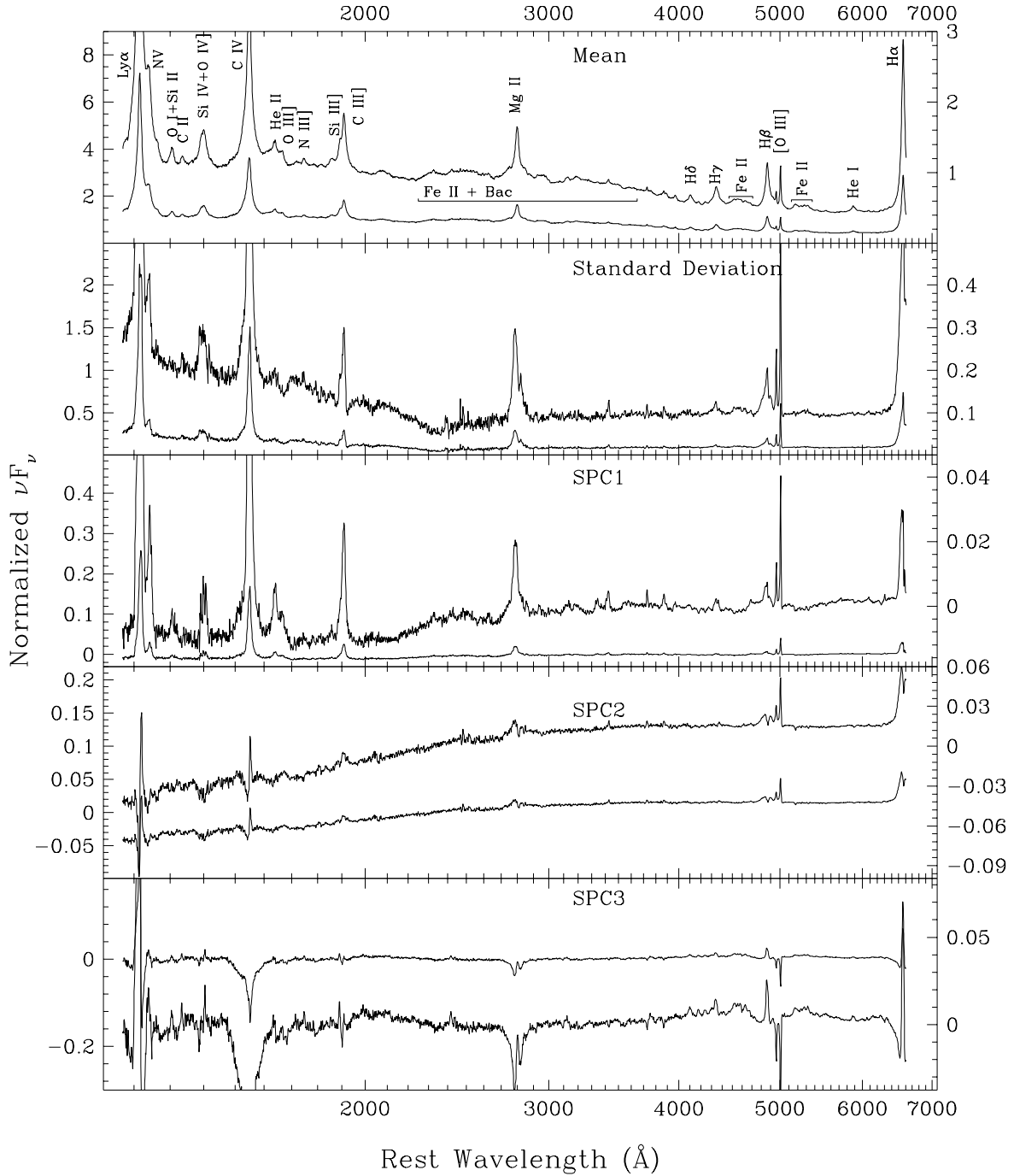


Fig. 11.— SPCA results for the UV-optical spectra of all 22 QSOs, i.e., including PG 1202+281 and the absorption-line QSOs, where the absorption regions are interpolated. Compare this figure with Fig. 3 that excludes these QSOs.

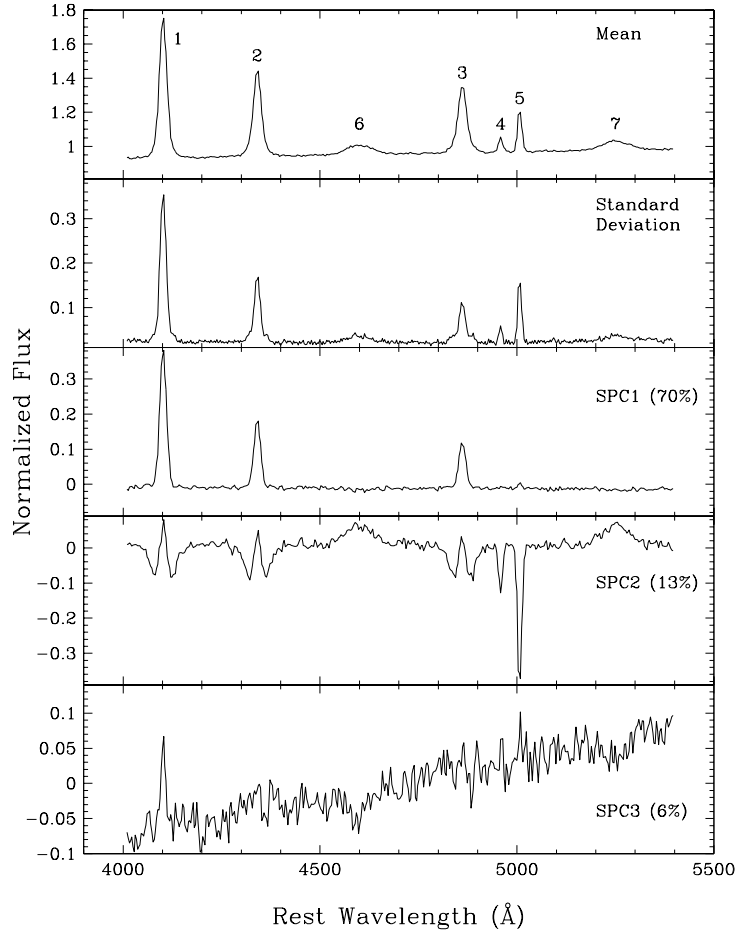


Fig. 12.— SPCA simulation with Gaussian profile. Three sets of relationships input via simulated spectra are separated into three principal components with small crosstalk (e.g., lines 1 and 5 in SPC3). Notice the “W” shape of lines 1, 2, and 3 in PC2. This indicates increasing width with increasing strength of lines 4 and 5. The numbers in parentheses represent the percentage of the intrinsic variance accounted for by each principal component.

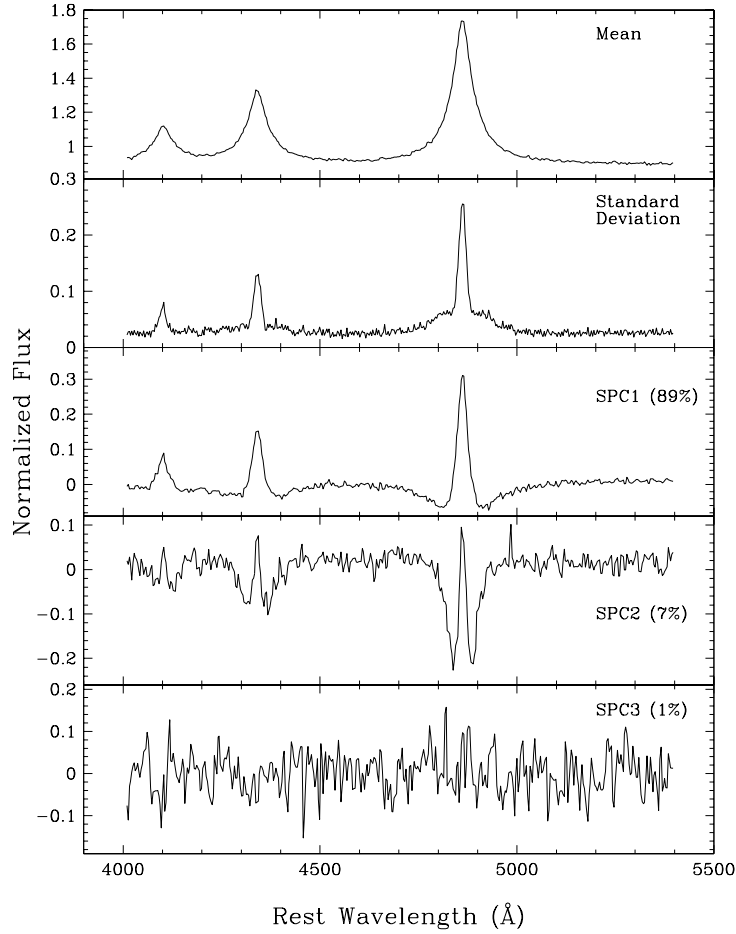


Fig. 13.— SPCA simulation with Lorentzian profiles. The non-linear relationship $\text{FWHM} \propto 1/I_p - c$ produces two dominant principal components. SPC1 shows that line width decreases with increasing line strength. SPC2 shows the effect of non-linear relationship among the flux bins as line width changes. The numbers in parentheses represent the percentage of the intrinsic variance accounted for by each principal component.